

การคาดการณ์การตอบสนองต่อคลื่นแผ่นดินไหวของดินโดยใช้
เทคนิคโคดาเวพอินเตอร์เฟอโรเมทรีบริเวณ
รายเลื่อนชานแอนเดรียสตอนใต้

นางสาวเพ็ญประภา วุฒิจักร
เลขประจำตัวนิสิต 513 27377 23

รายงานนี้เป็นส่วนหนึ่งของการศึกษาตามหลักสูตรปริญญาตรี
สาขาวิชาธรณีวิทยา ภาครหณีวิทยา คณะวิทยาศาสตร์
จุฬาลงกรณ์มหาวิทยาลัย ปีการศึกษา 2554

GROUND MOTION PREDICTION USING CODA-WAVE
INTERFEROMETRY FOR THE SOUTHERN
SAN ANDREAS FAULT

Miss Penprapa Wutthijuk

ID 513 27377 23

A REPORT IN PARTIAL FULFILLMENT OF THE REQUIREMENT
FOR THE DEGREE OF THE BACHELOR SCIENCE
DEPARTMENT OF GEOLOGY FACULTY OF SCIENCE
CHULALONGKORN UNIVERSITY

2011

____/____/____

Date of submit

____/____/____

Date of approval

.....
(Dr. Thanop Thitimakorn)

Senior Project Advisor

การคาดการณ์การตอบสนองต่อคลื่นแผ่นดินไหวของดินโดยใช้เทคนิคโคดาเวฟ
อินเตอร์เฟอร์โรเมทรี บริเวณรอยเลื่อนชานแอนเดรียสตอนใต้

นางสาวเพ็ญประภา วุฒิจักร

ภาควิชาธรณีวิทยา คณะวิทยาศาสตร์ จุฬาลงกรณ์มหาวิทยาลัย
โทรศัพท์: 0-8790-47401, อีเมล: penprapa_eay728@hotmail.com

บทคัดย่อ

การคาดการณ์การตอบสนองต่อคลื่นแผ่นดินไหวของแต่ละพื้นที่เป็นเรื่องที่มีความสำคัญ และเป็นประโยชน์อย่างมาก เพราะเราพบว่าแต่ละพื้นที่มีการตอบสนองต่อคลื่นแผ่นดินไหวที่ต่างกัน ทำให้มีอิทธิพลต่อการสั่นไหวที่จุดกำเนิดเดียวกัน แต่ละพื้นที่มีการตอบสนองต่อคลื่นแผ่นดินไหวดังกล่าวในลักษณะของการสั่นไหวที่มีความรุนแรงแตกต่างกัน ยิ่งไปกว่านั้น การคาดการณ์การตอบสนองต่อคลื่นแผ่นดินไหวของเขตพื้นที่เมืองใหญ่อย่างมหานครลօสแองเจลิสยัง เป็นเรื่องท้าทายของนักแผ่นดินไหววิทยา เพราะนอกจากพื้นที่ดังกล่าวจะเป็นที่ตั้งของมหานครขนาดใหญ่ มีความสำคัญทั้งในเชิงเศรษฐกิจและที่อยู่อาศัยของคนจำนวนมากแล้ว มหานครแห่งนี้ยังตั้งอยู่บนแหล่งตะกอนและอยู่ใกล้กับแนวการวางตัวของรอยเลื่อนชานแอนเดรียสตอนใต้ ด้วยเหตุนี้ บริเวณดังกล่าวจึงเป็นพื้นที่เสี่ยงที่จะเกิดแผ่นดินไหวได้ นอกจากนี้พบว่าผลของตะกอนในแหล่งยังทำให้เกิดการขยายตัวของคลื่นแผ่นดินไหวซึ่งจะทำให้ระดับการสั่นไหวมีความรุนแรงมากขึ้น งานวิจัยนี้จึงสนใจคาดการณ์การตอบสนองต่อคลื่นแผ่นดินไหวของพื้นที่例外ของลօสแองเจลิสและวอชิงตันดีซิท เมืองที่อยู่ติดกันและมีความสำคัญทางเศรษฐกิจและเชื้อชาติที่สูง

จากการศึกษางานวิจัยที่ผ่านมา พบว่าการตอบสนองต่อคลื่นแผ่นดินไหวของพื้นที่สามารถคำนวณได้จากพังก์ชันของกรีน ซึ่งพื้นที่ศึกษานี้มีการคำนวณพังก์ชันของกรีนจากไฮซ์มิคโนย์แล้ว แต่มีข้อจำกัดในเรื่องของการกระจายตัวของแหล่งกำเนิดคลื่นที่ไม่หลากหลาย งานวิจัยนี้จึงสนใจคำนวณพังก์ชันของกรีนจากคลื่นแผ่นดินไหวขนาดแมกนิทูด 7.2 และมีจุดศูนย์กลางที่บajaแคลิฟอร์เนียโดยใช้เทคนิคโคดาเวฟอินเตอร์เฟอร์โรเมทรี ซึ่งผลการศึกษาพบว่าเทคนิคนี้สามารถใช้คำนวณพังก์ชันของกรีนได้และพังก์ชันที่คำนวณได้มีสัดส่วนของสัญญาณต่อคลื่นรบกวนที่มากกว่าพังก์ชันที่คำนวณได้จากไฮซ์มิคโนย์ แสดงให้เห็นว่าพังก์ชันของกรีนที่คำนวณจากโคดาเวฟมีความถูกต้องแม่นยำมากกว่าและบางกรณีพบว่าผลรวมของพังก์ชันที่คำนวณได้จากโคดาเวฟและไฮซ์มิคโนย์ทำให้ได้พังก์ชันที่มีความถูกต้องมากขึ้น นอกจากนี้พังก์ชันของกรีนที่คำนวณจากเทคนิคโคดาเวฟอินเตอร์เฟอร์โรเมทรียังสามารถนำมาใช้สร้างแผนที่แสดงระดับการสั่นไหวของพื้นที่แคลิฟอร์เนียต่อไปได้ กรณีเกิดแผ่นดินไหวขนาดแมกนิทูด 7 บริเวณรอยเลื่อนชานแอนเดรียสตอนใต้

Keywords: ground motion prediction, coda-wave interferometry

Ground Motion Prediction Using Coda-Wave Interferometry for the Southern San Andreas Fault

Miss Penprapa Wutthijuk

Department of Geology, Faculty of Science, Chulalongkorn University

Tel: 0-8790-47401, E-mail: penprapa_eay728@hotmail.com

ABSTRACT

Ground motion prediction in urban areas that are under the threat of major earthquakes, such as Los Angeles, is a challenge for seismic hazard analysis. The effect of complex sedimentary basins is a source of particular concern for simulating wave propagation here. Previous works developed a new approach that directly accounts for elastic and anelastic effects, through computing the Green's function using seismic noise. However, this technique is limited because the distribution of the noise sources in southern California is not homogeneous.

This project used coda-wave interferometry of the M7.2 El Mayor-Cucapah aftershock to extract the Green's function for stations along the southern San Andreas fault. By stacking the Green's function, we found that Green's function can be extracted from coda-wave interferometry and has higher signal to noise ratio than seismic noise Green's function that implied more accurate Green's function. Furthermore, the combination of both would greatly enhance the accuracy of the retrieved Green's function. Finally, obtained coda-wave Green's function can be used to predict ground motion in Los Angeles sedimentary basin as a response to M7+ earthquake on the San Andreas fault.

Keywords: ground motion prediction, coda-wave interferometry

ACKNOWLEDGEMENTS

This project would have not been achieved without the support of many people. I owe a great many thanks to a great many people who help and encourage me during the completing of this project.

The special thank goes to my helpful advisor, Dr.Thanop Thitimakorn, and co-advisors, Dr.Santi Pailoplee, Prof.Gregory C. Beroza and Marine Denolle. The supervision and support that they gave truly help the progression and smoothness of the doing this senior project. My deep sense of gratitude to Assoc. Prof. Visut Pisutha-Arnond, Miss Malatee Taiyaqupt and Prof. Jerry M. Harris who gave a great opportunities to me to attend the valuable program like the SURGE (Summer Research in Geosciences and Engineering) program at Stanford University. My grateful thanks also go Department of Geology, Chulalongkorn University, Department of Geophysics, Stanford University and Chevron Thailand for supporting me participating this program. I deeply appreciate your kindness. I also wish to express my thanks to SURGE people who shared knowledges and experiences with me from the initial to final time of SURGE program.

My deepest thanks to all of my education lecturers through my 4 years in Department of Geology, Faculty of Science, Chulalongkorn University, Assoc. Prof. Dr.Punya Charusiri, Assist. Prof.Virote Daorerk, Assoc. Prof. Dr.Visut Pisutha-Arnond, Assist. Prof. Dr.Somchai Nakapadungrat, Assist. Prof. Dr.Sombat Yumuang, Assist. Prof. Dr.Chakrapan Sutthirat, Assist. Prof. Dr.Thasinee Charoentitirat, Assoc. Prof. Dr.Montri Choowong, Dr.Vichai Chutakositkanon, Dr.Yoshio Sato, Dr.Pitsanupong Kanjanapayont, Dr.Thanop Thitimakorn, Dr.Santi Pailoplee, Dr.Akaneewut Chabangbon, Miss Malatee Taiyaqupt and Miss Bussarasiri Thana, for giving me the knowledge about geology, geophysics and also experiences.

I wish to express my thanks to my family who has always been there for me whenever I need them, the encouragement they give to keep me going and their love to empower me that never fails all the time. Thank you.

I would also thank my geology classmate, GEO'52, without whom this project would have been a distant reality and my life would not be complete.

CONTENTS

	Page
ABSTRACT IN THAI.....	iv
ABSTRACT IN ENGLISH.....	v
ACKNOWLEDGEMENTS.....	vi
CONTENTS.....	vii
LIST OF TABLES.....	ix
LIST OF FIGURES.....	x
CHAPTER I INTRODUCTION.....	1
1.1 General Statement.....	1
1.2 Objectives.....	7
1.3 Scope of Work.....	7
1.4 Study Area.....	7
1.5 Expected Results.....	11
CHAPTER II LITERATURE AND THEORY.....	12
2.1 Literature Review.....	12
2.2 Theory.....	20
2.2.1 Ground Motion.....	20
2.2.2 Green's Function.....	20
2.2.3 Crosscorrelation.....	21
2.2.4 Seismic Interferometry.....	24
2.2.5 Coda-wave.....	26
2.2.6 Fast Fourier Transform.....	26
2.2.7 Seismic Noise.....	27
CHAPTER III METHODOLOGY.....	28
Methodology.....	28
CHAPTER IV RESULT AND INTEPRETATION.....	33
Result and Interpretation.....	33

	Page
CHAPTER V DISCUSSION AND CONCLUSION.....	46
5.1 Discussion and Conclusion.....	46
5.2 Recommendation.....	49
REFERENCES.....	50
APPENDICES.....	53
APPENDIX A The C++ Script to Remove Instrument Response.....	54
APPENDIX B The MATLAB Script to Pick Time Window of Coda-wave.....	55

LIST OF TABLES

	Page
CHAPTER I INTRODUCTION	
Table 1.1 M7.2 Sierra El Mayor Earthquake Details.....	10
CHAPTER II LITERATURE AND THEORY	
Table 2.1 30-year probability of M6.7 events on the Type-A faults, rounded to the nearest percent.....	19

LIST OF FIGURES

	Page
CHAPTER I INTRODUCTION	
Figure 1.1 The model shows earthquake system.....	1
Figure 1.2 Ground shacking is amplified in soft sediments and dampened in hard rock.....	2
Figure 1.3 The effect of 1987 Edgecumbe earthquake.....	3
Figure 1.4 The effect of 2004 earthquake in Japan and 1994 Northridge earthquake.....	3
Figure 1.5 Map of southern California that shows the location of Los Angeles.....	4
Figure 1.6 The model of earthquake system represents the different earth response and shaking level in different location.....	5
Figure 1.7 Location of Los Angeles sedimentary basin (red curve) and the directions of coda-wave and seismic noise.....	6
Figure 1.8 Geological Map of California.....	8
Figure 1.9 Map of modern San Andreas fault.....	9
Figure 1.10 Intensity map of M7.2 Sierra El Mayor.....	11
CHAPTER II LITERATURE AND THEORY	
Figure 2.1 The average correlation function.....	12
Figure 2.2 Map showing the station location and Cross- correlations of vertical-component records.....	14
Figure 2.3 Analysis of broadband (0.008–0.07 Hz) cross-correlations.....	15
Figure 2.4 Definition of the geometric variables for the waves that travel from a scatterer.....	16
Figure 2.5 Location map for the TeraShake simulations.....	18
Figure 2.6 Source characteristics and crustal structure for the TeraShake simulations.....	18

	Page
Figure 2.7 Maximum RMS PGV for SE-NW1 and SE-NW2 scenarios.....	19
Figure 2.8 A recording of ground motion.....	20
Figure 2.9 Interferometric construction of a virtual source.....	21
Figure 2.10 Alternative, more Earth-like models for which the process in Figure 2.9... 23	
Figure 2.11 A 1D example of direct-wave interferometry.....	24
Figure 2.12 As in Figure 2.11 but this time for a leftward-traveling impulsive plane wave.....	25
Figure 2.13 Seismogram shows body and coda wave.....	26
CHAPTER III METHODOLOGY	
Figure 3.1 Locations of Los Angeles sedimentary basin, seismic broadband stations and earthquake.....	28
Figure 3.2 Methodology flowchart.....	32
CHAPTER IV RESULT AND INTERPRETATION	
Figure 4.1 Locations of seismic broadband stations around southern California that recorded seismic wave of M7.2 El Mayor earthquake.....	33
Figure 4.2 Locations of seismic broadband station CI_ADO and earthquake data... 34	
Figure 4.3 Locations of seismic broadband station CI_ALP and earthquake data.... 34	
Figure 4.4 The seismic data of M 7.2 Sierra El Mayor earthquake recorded by seismic broadband station CI_ADO before and after picke time window of Coda- wave.....	35
Figure 4.5 The seismic data of M 7.2 Sierra El Mayor earthquake recorded by seismic broadband station CI_ALP before and after picke time window of Coda- wave.....	35
Figure 4.6 Locations of seismic station CI_LDF and CI_BHP and the characteristic of Green's function between these two stations.....	36
Figure 4.7 Locations of seismic station CI_USC and CI_BHP and the characteristic of Green's function between these two stations.....	36

	Page
Figure 4.8 Locations of seismic station CI_DPP and CI_BTC and the characteristic of Green's function between these two stations.....	37
Figure 4.9 Locations of seismic station CI_EML and CI_DNR and the characteristic of Green's function between these two stations.....	37
Figure 4.10 Map shows location of broadband station that represents the Symmetric Green's function.....	38
Figure 4.11 Locations of seismic station CI_BAR and CI_ALP and the characteristic of Green's function between these two stations.....	39
Figure 4.12 Locations of seismic station CI_BBS and CI_ALP and the characteristic of Green's function between these two stations.....	39
Figure 4.13 Map shows location of broadband station that represents the Anti-symmetric causal Green's function.....	40
Figure 4.14 Locations of seismic station CI_IRM and CI_BTC and the characteristic of Green's function between these two stations.....	41
Figure 4.15 Locations of seismic station CI_MGE and CI_IRM and the characteristic of Green's function between these two stations.....	41
Figure 4.16 Map shows location of broadband station that represents the Anti-symmetric anti-causal Green's function.....	42
Figure 4.17 Map shows location of broadband station that represents the complementary Green's function.....	43
Figure 4.18 Map shows location of broadband station that represent the example of Green's function comparison of coda-wave Green's function and seismic noise Green's function in case the source is at station BFS.....	44
Figure 4.19 Hazard map or ground motion map represents the level of ground shaking in case of M7+ occur along the southern San Andreas fault.....	45

	Page
CHAPTER V DISCUSSION AND CONCLUSION	
Figure 5.1 Map shows location of broadband station that represents the Symmetric Green's function, Anti-symmetric causal Green's function and Anti- symmetric anti-causal Green's function.....	47
Figure 5.2 Hazard map or ground motion map represents the level of ground shacking that is not follow the geometric spreading.....	48

CHAPTER I

INTRODUCTION

1.1 General Statement

Earthquakes are natural ground motions caused as the earth releases energy. The earthquake energy comes from the stresses of plate tectonics. As plates move, the rocks on their edges deform and take up strain until the weakest point, a fault, ruptures and releases the strain. Tectonic earthquakes occur anywhere in the earth where there is sufficient stored elastic strain energy to drive fracture propagation along a fault plane. When the force of the moving blocks finally overcomes the friction of the jagged edges of the fault and it unsticks, all that stored up energy is released. The energy radiates outward from the fault in all directions in the form of seismic waves like ripples on a pond. The seismic waves shake the earth as they move through it, and when the waves reach the earth's surface, they shake the ground and anything on it, like our houses and us.

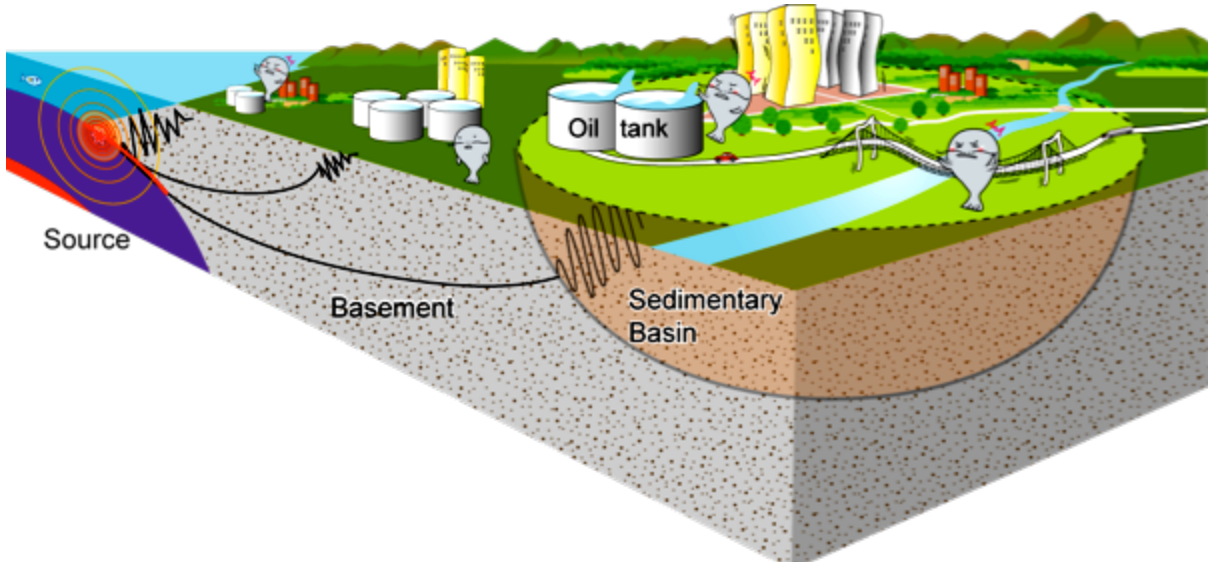


Figure 1.1 The model shows earthquake system. (AIST, 2010)

When we discussed earthquake intensity we discussed some of the basic factors that affect the amplitude and duration of shaking produced by an earthquake and as you are aware, the shaking caused by seismic waves can cause damage buildings or cause

buildings to collapse. The level of damage done to a structure depends on the amplitude and the duration of shaking. The amplitudes are largest close to large earthquakes and the duration generally increases with the size of the earthquake. Regional geology can affect the level and duration of shaking but more important are local site conditions. Although the process can be complicated for strong shaking, generally shaking in soft sediments is larger and longer than when compared with the shaking experienced at a hard rock site.

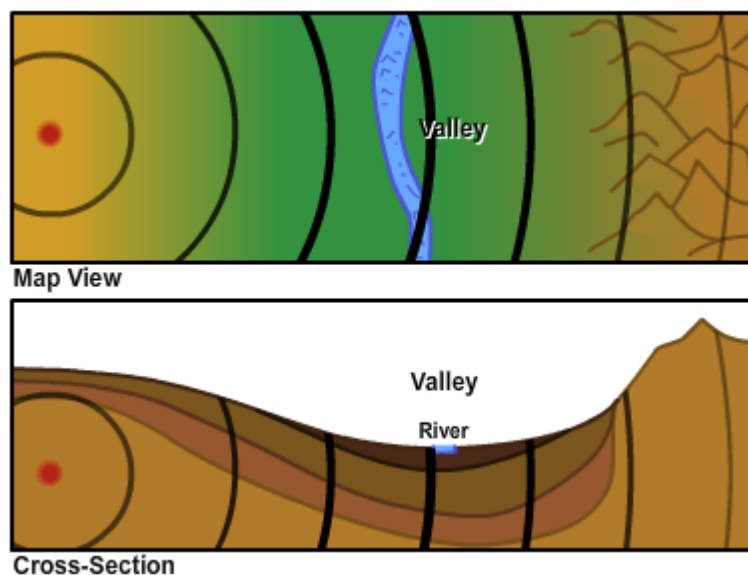


Figure 1.2 Ground shacking is amplified in soft sediments and damped in hard rock. (USGS, 2009)

Due to the different of earthquake size, distance from fault, site and regional geology, the shaking hazard is different.



Figure 1.3 The effect of 1987 Edgecumbe earthquake. The land to the northwest of the Edgecumbe Fault sank by up to 2 meters. The fault ruptured the surface, forming a seven-kilometer-long rift across the countryside, and causing widespread damage from shaking.

<<http://www.teara.govt.nz/en/earthquakes/2/3>>



Figure 1.4 The effect of 2004 earthquake in Japan (left) <http://skoola.com/read_news.php?id=190> and the effect of 1994 Northridge earthquake (right). <<http://mceer.buffalo.edu/research/resilience/>>

Because of the different shaking hazard in different area, the effects to people, building and also economic are different. If the earthquake occurs in big metropolitan area, such as Los Angeles, it will cause the large effect to people and economic. Los Angeles, the project study area, is located on southern California that also the location of famous active fault, San Andreas Fault.

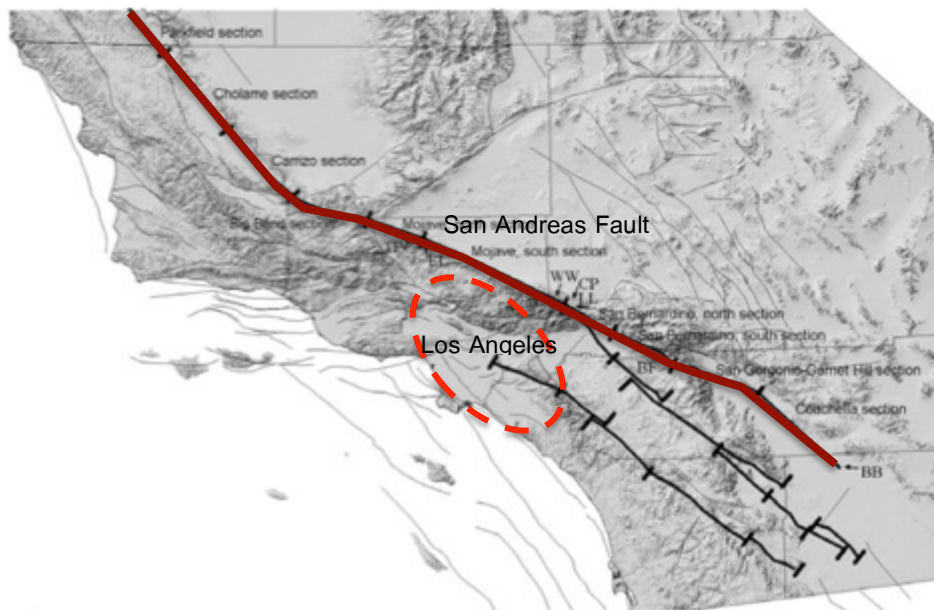


Figure 1.5 Map of southern California that shows the location of Los Angeles (red ellipse) and San Andreas fault (red line). (USGS, 2008)

Ground motion prediction in urban areas that are under the threat of major earthquakes, such as Los Angeles, is a challenge for seismic hazard analysis. The effect of complex geological structures, such as in sedimentary basins, on ground motion prediction is a source of particular concern for simulating wave propagation.

$$u(t) = s(t) * g(t)$$

$$\bullet = \Delta + \square$$

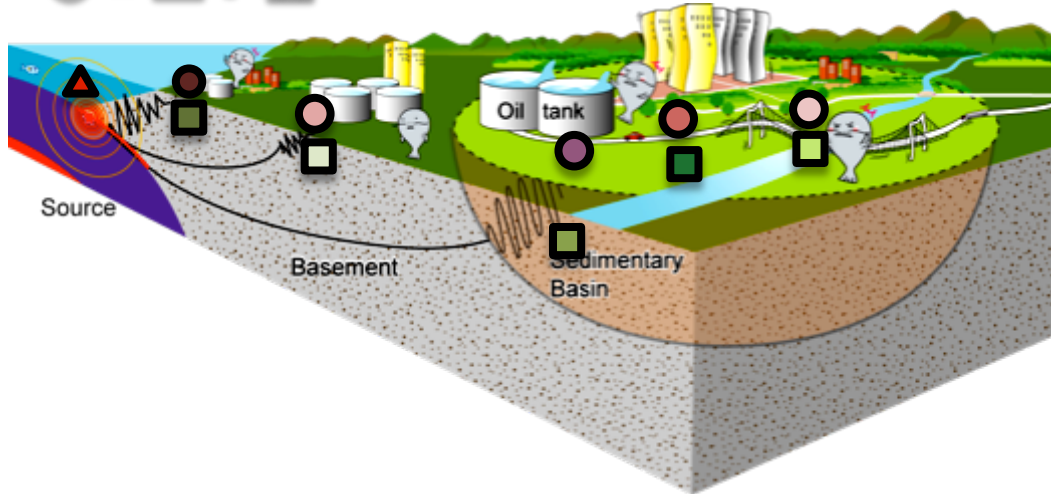


Figure 1.6 The model of earthquake system (AIST, 2010) represents the different earth response and shaking level in different location. (triangular shows the seismic source, circles show the level of ground shaking and squares show the response of the earth at each location)

One reason that causes the different shaking level in each area is the different of earth's response when the seismic waves propagate through the earth surface. If we know the response of the earth due to the propagated seismic wave in each area, we can predict the ground motion in that area.

The response of the earth to an impulse force is represent by Green's function. According to Lobkis and Weaver (2001, 2002) showed that the Green's function could be extracted from the correlation properties of diffuse fields. In seismology, two kinds of fields are usually considered as diffuse: the seismic noise and the scattered waves of the coda. Seismic noise has the advantage that it is easy to record because it is ubiquitous in many regions of the earth and active 24-hours a day, and has important low frequency components (Shapiro et al., 2005; Zhang et al., 2010). Prieto and Beroza (2008) developed a new approach that directly accounts for elastic and anelastic effects, through computing the Green's function using the seismic noise. However, the use of seismic noise has some limitations because the noise source is non-uniform. In the case of southern California, the source of seismic noise is primarily from the Pacific Ocean,

which is located to the west of the Los Angeles Basin. Thus, for this geometry it is challenging to extract an accurate, unbiased Green's function using seismic records.

This project concentrate on coda waves, since they are produced by a known source and they have been shown to result from multiple scattering in the Earth's lithosphere. Campillo and Paul (2003) showed that the use of field-to-field correlation to retrieve the Green's function is valid not only in the extremely controlled and favorable condition of the laboratory but also with natural signals produced by earthquakes.

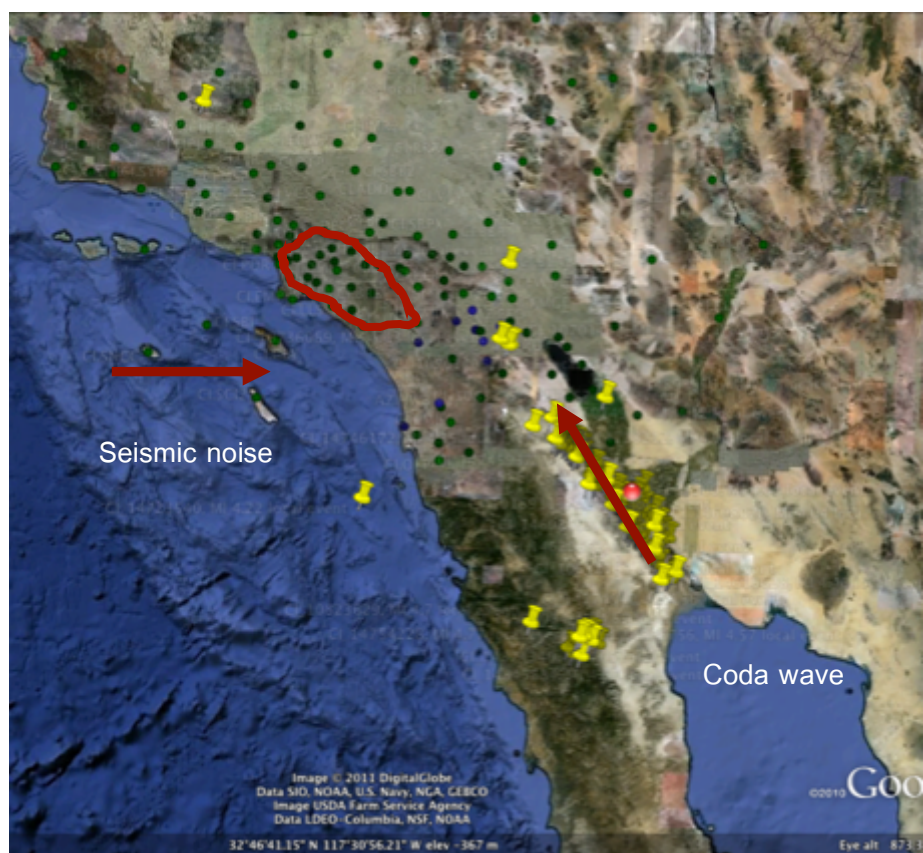


Figure 1.7 Location of Los Angeles sedimentary basin (red curve) and the directions of coda-wave and seismic noise <<http://www.google.com/earth/download/ge/agree.html>>

We present here an application for improved ground motion prediction for the geologically complex Los Angeles Basin, using coda- wave interferometry on the aftershock of M7.2 Cucapah earthquake for stations near the southern San Andreas fault.

1.2 Objectives

1. Extract coda-wave Green's functions that use to predict amplification of the passing waves in this sedimentary basins.
2. Estimate the ground motion of southern California.

1.3 Scope of Work

For this study, we propose to use the aftershock sequence of the large, Mw=7.2, El Mayor-Cucapah earthquake of April 4th, 2010, to compute the Green's function for stations along the southern San Andreas fault with coda-wave interferometry and compare the results with Green's functions determined from the seismic noise.

1.4 Study Area

The unique landscape of southern California is extremely varied, with high mountains, expansive deserts, sandy and rocky beaches, brushy hills, and broad river valleys in close proximity to each other. Eight physiographic provinces are represented in the varied terrain of southern California: the southern Sierra Nevada, the southern Coast Ranges, the southern Great Valley, the Transverse Ranges, the Peninsular Ranges, the Colorado Desert, the Mojave Desert, and the main part of the Basin and Range.

A geologic map portrays the distribution of rock types and ages at the surface along with information about the orientation of rock bodies and the location and extent of geological structures such faults and folds. The rocks of southern California are extremely varied. Igneous rocks are exposed in many places and include Mesozoic plutonic rocks similar to granite and Cenozoic volcanic rocks such as basalt, rhyolite, and tuff. Sedimentary rocks are also widespread including Mesozoic and Cenozoic shale and sandstone of marine origin along with thick sequences of Cenozoic terrestrial sedimentary rocks. Metamorphic rocks are represented primarily by schist and gneiss of either Precambrian or Mesozoic age.

The mountains of southern California are relatively young and have formed through normal faulting under tension in the Basin and Range, folding and reverse faulting generated by compression in the Transverse Range, and through oblique faulting related to shear stress in several places along the San Andreas fault zone.

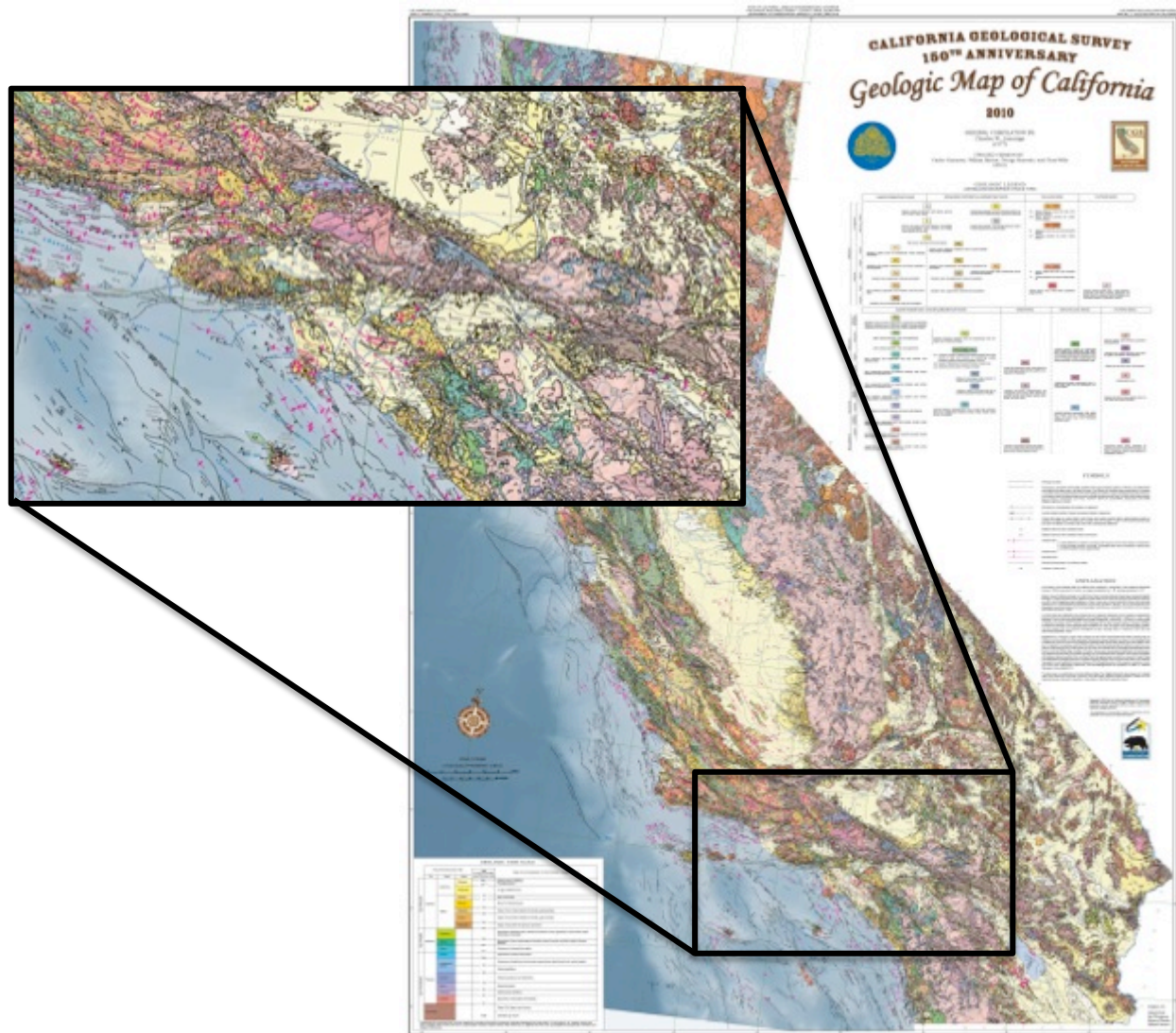


Figure 1.8 Geological Map of California that the map in black rectangular is the area of southern California, the study area of this project.

< http://www.conservation.ca.gov/cgs/cgs_history/Pages/2010_geologicmap.aspx >

The San Andreas fault system, comprised of several different fault zones, is a complex system of mostly strike-slip faults that extends for more than 1,300 km from the Gulf of California coast. Within this zone, there are hundreds of strike-slip faults, including of course the San Andreas itself. The dominant motion on the faults is right-lateral, and their cumulative effect is to displace the silver of California west of the fault system to the northwest relative to the North American plate on the opposite side. The rate of displacement between the Pacific and North American plates varies somewhat along the

boundary, but averages about 5 cm/yr. Since its inception 28 million years ago, total right-lateral offset is slightly less than 470 kilometers. However, no single fault within the San Andreas system accommodates all of the motion between the North American and Pacific plates. In fact, neither does the San Andreas system as a whole. Right-lateral faults and shear zones related to the Pacific-North American plate boundary extend as far inland as western Nevada. Thus, the San Andreas fault system is the primary manifestation of the modern transform plate boundary, but is not precisely synonymous with it.



Figure 1.9 Map of modern San Andreas fault

< http://geomaps.wr.usgs.gov/archive/socal/geology/geologic_history/san_andreas_history.html >

The coda-waves that used in this project come from seismic recorded data of M7.2 earthquake. The M7.2 Sierra El Mayor earthquake of Sunday April 4th 2010, occurred in northern Baja California, approximately 40 miles or 65 km south of the Mexico-USA border at shallow depth along the principal plate boundary between the North American and Pacific plates. At the latitude of the earthquake, the Pacific plate moves northwest with respect to the North America plate at about 1.8 inches per year. The principal plate boundary in northern Baja California consists of a series of northwest-

trending strike-slip (transform) faults that are separated by pull-apart basins. The faults are distinct from, but parallel to, strands of the San Andreas fault system. The April 4 main-shock occurred along a strike-slip segment of the plate boundary that coincides with the southeastern part of the Laguna Salada fault system. It is a complex event that may have begun with east-down motion along faults on the eastern edge of the Sierra El Mayor, then progressed to the northwest with oblique slip, that is, a combination of lateral shift to the right and also east-down motion. Overall, the location and focal-mechanism of the earthquake are consistent with the shock having occurred on this fault system. Aftershocks appear to extend in both directions along this fault system from the epicenter of the 4 April 2010 event. The aftershock zone extends from near the northern tip of the Gulf of California to 6 miles northwest of the Mexico-USA border.

Table 1.1 M7.2 Sierra El Mayor Earthquake Details (USGS, 2010)

Magnitude	7.2
Date-Time	Sunday, April 04, 2010 at 22:40:42 UTC Sunday, April 04, 2010 at 03:30:42 PM at epicenter
Location	32.259°N, 115.287°W
Depth	10 km
Region	Baja California, Mexico
Distances	50 km SSE of Mexicali, Baja California, Mexico 50 km WSW of San Luis Rio Colorado, Sonora, Mexico 65 km SSE of El Centro, California 2145 km NW of MEXICO CITY, D.F., Mexico

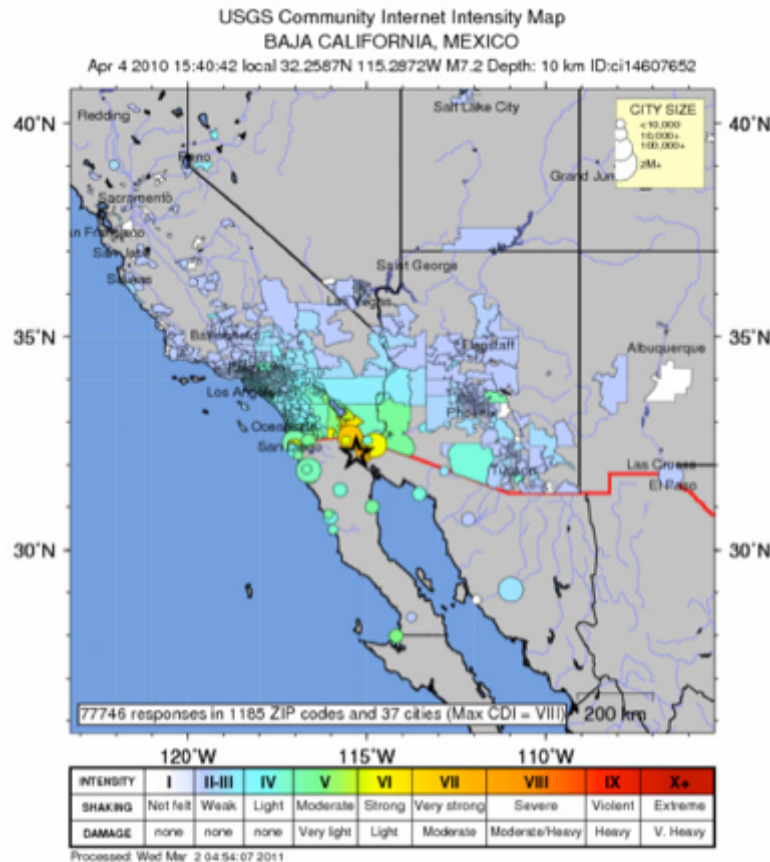


Figure 1.10 Intensity map of M7.2 Sierra El Mayor

< <http://earthquake.usgs.gov/earthquakes/dyfi/events/ci/14607652/us/index.html> >

1.5 Expected Results

1. This method will allow us to retrieve the Green's function in between seismic stations with preserving the relative amplitude information.
2. The result will improve the seismic noise Green's function amplitude stability.
3. The extracted Coda-wave Green's function will be able to estimate the ground motion or hazard map of southern California especially of Angeles sedimentary basin.

CHAPTER II

LITERATURE AND THEORY

2.1 Literature Review

Lobkis and Weaver (2001) studied the emergence of Green's function in the correlations of a diffuse field. They found that a diffuse acoustic field is shown to have correlations equal to the Green's function of the body. The literatures of the last several years on diffuse ultrasonic fields in solid, on diffuse vibrations in structural acoustics, and on diffuse seismic fields in the earth's crust has largely neglected the field's phase, and focused instead on the field's spectral energy density. This is for good reason; fields which have reflected or scattered many times from specimen surfaces or inclusions resist detailed analysis. The temporal cross-correlation function between the signals received simultaneously in two distinct transducers is shown to be the signal which one transducer would receive when the other is given an impulsive excitation. The correlation displays all travel paths between the two points, including those with multiple reflections.

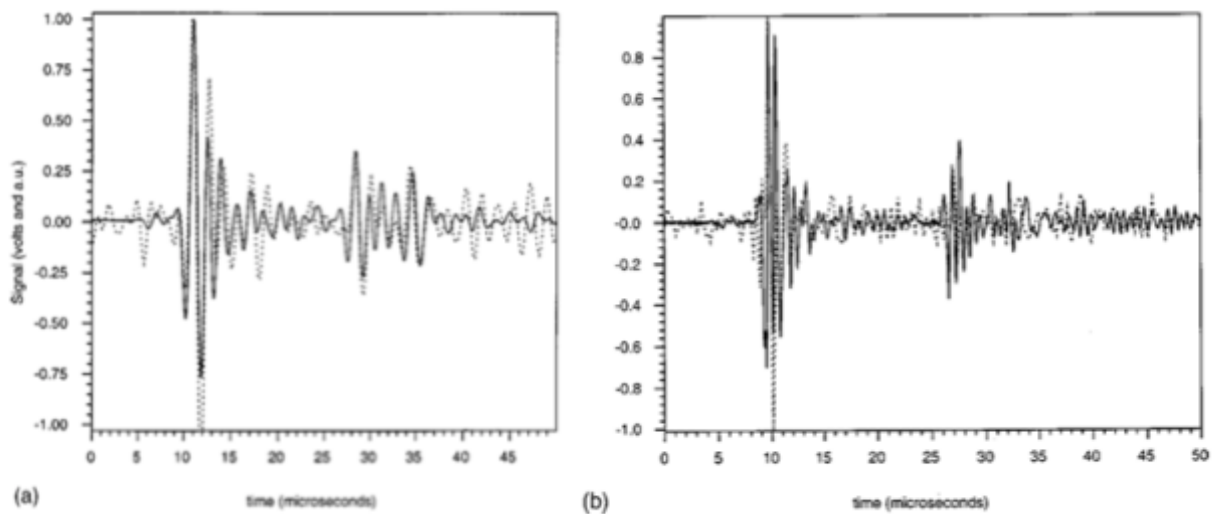


Figure 2.1 (a) The average correlation function recovered from 190 ms of data generated by eight distinct positions of the source s (dashed line) is compared with the direct pitch-catch signal (solid line). Each waveform has been low-pass filtered at 900 kHz. The average correlation function without low-pass filtering, as recovered from 128 ms of data generated by eight distinct positions of the source s (dash line) is compared with the direct pitch-catch signal (solid line). (Lobkis and Weaver, 2001)

Lobkis and Weaver (2002) studied the emergence of the Green's function in the correlations of a diffuse field: pulse-echo using thermal phonons. They found that a diffuse field is not devoid of phase information, but has a correlation function equal to the Green's function. More specifically, the cross-correlation between diffuse signals in two transducers is very nearly equal to the direct response of one transducer to an impulse applied to the other. This is true whether the diffuse field is one that was created by a distant source, or (if the detectors are sufficiently sensitive) created by thermal fluctuations in the specimen.

Shapiro and Campillo (2004) studied the emergence of broadband Rayleigh waves from correlations of the ambient seismic noise. They demonstrate that the coherent information about the earth structure can be extracted from the ambient seismic noise. They compute cross-correlations of vertical component records of several days of seismic noise at different pairs of stations separated by distances from about one hundred to more than two thousand kilometers. Coherent broadband dispersive wavetrains clearly emerge with group velocities similar to those predicted from the global Rayleigh-wave tomographic maps that have been constrained using ballistic surface waves. Those results show that coherent Rayleigh waves can be extracted from the ambient seismic noise and that their dispersion characteristics can be measured in a broad range of periods.

Recent developments in acoustics and seismology suggest an alternative method to measure the elastic response of the Earth by extracting the Green function from the diffuse or random wavefields. Contrary to ballistic waves, fully diffuse wavefields are composed of waves with random amplitudes and phases but propagating in all possible directions and, therefore, contain the information about any possible path that can be extracted by computing cross-correlations between pairs of receivers. A simple demonstration of this property is based on a modal representation of a diffuse wavefield inside an elastic body

$$\emptyset(x, t) = \sum_n a_n u_n(x) e^{i\omega_n t} \quad (2.1)$$

where x is position, t is time, u_n and w_n are eigenfunctions and eigenfrequencies of the real earth, and a_n are modal excitation functions. An important property of the diffuse field is that the modal amplitudes are uncorrelated random variables.

$$\langle a_n a_m^* \rangle = \delta_{nm} F(\omega_n) \quad (2.2)$$

where $F(w)$ is the spectral energy density. Because the cross-terms disappear in average due to equation above, the correlation between the fields at locations x and y becomes simply.

$$C(x, y, \tau) = \sum_n F(\omega_n) u_n(x) u_n(y) e^{-i\omega_n \tau} \quad (2.3)$$

The expression equation above differs only by an amplitude factor F from an actual Green function between points x and y . This result reminds of the fluctuation-dissipation theorem. Its very important implication is that the Green function between two locations (or at least, the arrival times of the different wave-trains) can be extracted from the diffuse field with a simple field-to-field correlation taken over sufficiently long time.

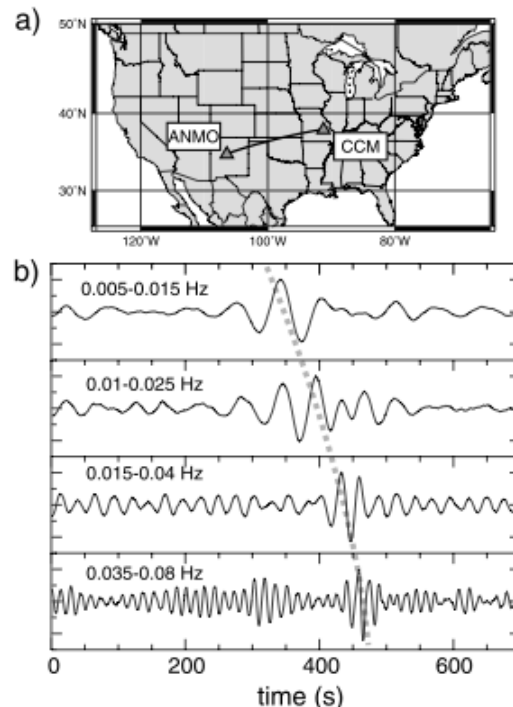


Figure 2.2 (a) Map showing the station location. (b) Cross- correlations of vertical-component records bandpass with different filters as indicated in top left corners of each frame. Gray dotted line emphasizes the dispersion of the emerging signal. (Shapiro and Campillo, 2004)

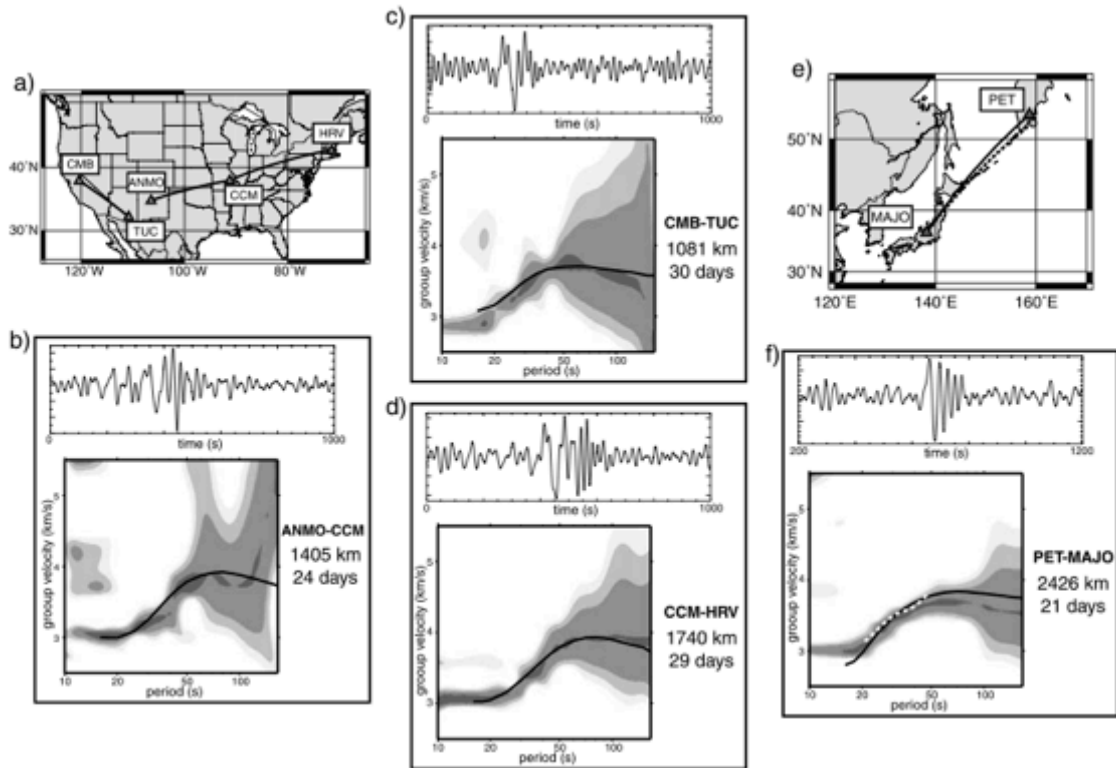


Figure 2.3 Analysis of broadband (0.008–0.07 Hz) cross-correlations computed for four pairs of stations from the continuous 1SPS vertical component channel recorded between January 10 and February 8, 2002. (a) Maps showing locations of stations in US. (b)–(d) results for three pairs of stations in US. (e) Map showing location of stations in North Western Pacific. (f) Results for stations PET and MAJO. For each pair of stations, the upper frame show the cross- correlation that has been high-pass filtered at 0.05 Hz to emphasize the long-period part of the emerging signal. The lower frame shows the comparison of a period group-velocity diagram computed from this cross-correlation with a dispersion curve (solid black line) predicted for the corresponding inter-station path from global Rayleigh-wave group velocity tomographic maps of computed from the ballistic surface waves. For each pair of stations, we indicate the inter-station distance and the total duration of the noise records available. For the path PET-MAJO, we also compare the period- group velocity diagram computed from the cross-correlation with the group-velocity dispersion curve (dotted white line) measured from an earthquake located near the coast of Kamchatka and recorded at MAJO.

(Shapiro and Campillo, 2004)

Snieder (2004) studied the methodology to extract the Green's function from the correlation of coda-wave. The Green's function of waves that propagate between two receivers can be found by cross-correlating multiply scattered waves recorded at these receivers. This technique obviates the need for a source at one of these locations, and is

therefore called passive imaging. Passive imaging is a technique wherein waves recorded at two receiver locations are correlated to give the Green's function that describes the direct wave propagation between these receivers. The tail of multiply scattered waves is called the "coda," after the Latin word for tail. Coda waves are effective for monitoring temporal changes in media. Using coda waves to determine the Green's function is useful because it provides information on wave propagation between two points in space without the need for a source at either of these two points. The Green's function thus obtained can be used to form an image of the medium. Passive imaging has been used in seismic exploration, helioseismology, and ultrasonic with either an active source or thermal noise that excites the coda. Numerical experiments have shown that passive imaging can be used both in closed and in open systems.

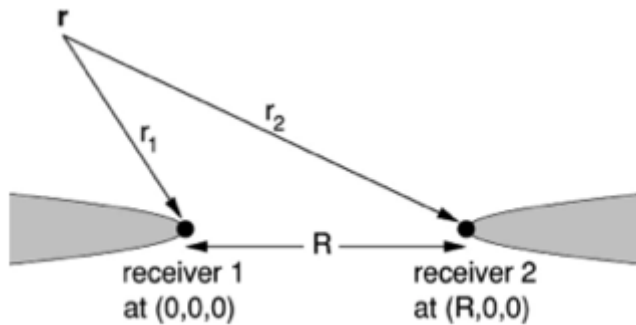


Figure 2.4 Definition of the geometric variables for the waves that travel from a scatterer at location r to two receivers. The shaded regions indicate the region of constructive interference. (Snieder , 2004)

$$C(\omega) = 8\pi^2 \overline{|S(\omega)|^2} \left(\frac{c}{i\omega} \right) \times \left(-\frac{e^{ikR}}{4\pi R} \int_{-\infty}^0 n dx - \frac{e^{-ikR}}{4\pi R} \int_R^\infty n dx \right) \quad (2.4)$$

The term $-\frac{e^{ikR}}{4\pi R}$ is the Green's function that accounts for the waves that propagate between the receivers; this term comes from the integration over $x < 0$. The second term $-\frac{e^{-ikR}}{4\pi R}$, which comes from the integration over $x > R$, is the advanced Green's function. The retarded Green's function comes from the waves that propagate from receiver 1 to receiver 2 and correlate for a positive lag time $\tau < 0$. The factor $\frac{1}{i\omega}$, which corresponds to an integration in the time domain, comes from the stationary phase evaluation of the x and y integrals.

As shown in equation above, the ballistic wave Green's function can be obtained by a cross correlation of the waveforms at two receivers. By using the correlations that are hidden in the coda waves, the destructive interference of waves radiated from scatterers away from the receiver line, and the constructive interference of scattered waves that propagate along the receiver line makes passive imaging an effective technique for extracting the ballistic wave Green's function between two points without using a source at either of these points.

Olsen *et al* (2006) studied the strong shaking in Los Angeles expected from southern San Andreas earthquake. The right-lateral, strike-slip San Andreas fault has produced a history of large ($\sim M8$) earthquakes most recently the 1906 event with tremendous damage to San Francisco. South of the 1906 rupture, the 1857 (El Cajon) earthquake ruptured the 360 km long stretch from Parkfield to Wrightwood. However, the two segments of the San Andreas fault south of the 1857 rupture, the San Bernardino Mountains segment and the Coachella Valley segment, have not seen a major event since 1812 and about 1690, respectively. The average recurrence intervals for large earthquakes with surface rupture on these segments are $146 + 91\text{-}60$ yrs and 220 ± 13 yrs, respectively. A major component of the seismic hazard in southern California and northern Mexico comes from a large earthquake on this part of the San Andreas fault. Since no strike-slip earthquake of similar or larger magnitude has occurred since the first deployment of strong motion instruments in southern California, there is a large uncertainty of the ground motions expected from such event. The southernmost San Andreas fault has a high probability of rupturing in a large (greater than magnitude 7.5) earthquake sometime during the next few decades.

To reduce this uncertainty we have carried out some of the largest and most detailed earthquake simulations completed to date (TeraShake), in which we model ground motions expected from a large earthquake on the southern San Andreas fault. New simulations show that the chain of sedimentary basins between San Bernardino and downtown Los Angeles form an effective waveguide that channels Love waves along the southern edge of the San Bernardino and San Gabriel Mountains. Earthquake scenarios with northward rupture, in which the guided wave is efficiently excited, produce unusually

high long-period ground motions over much of the greater Los Angeles region, including intense, localized amplitude modulations arising from variations in waveguide cross-section.



Figure 2.5 Location map for the TeraShake simulations. The red rectangle depicts the simulation area. The black rectangle depicts a section of the Los Angeles basin. The dotted line depicts the part of the San Andreas Fault that ruptured in the TeraShake simulations. (Olsen *et al*, 2006)

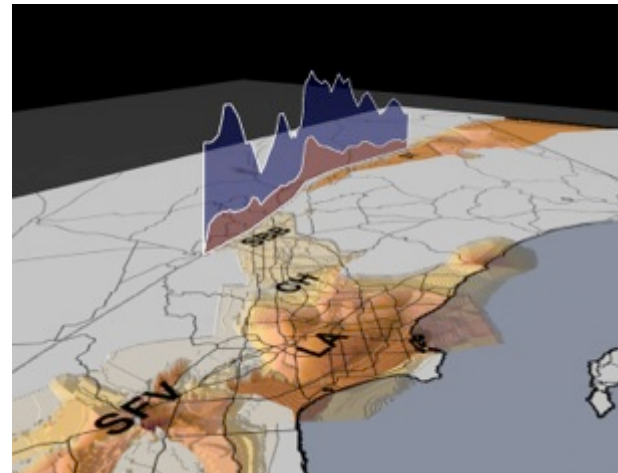


Figure 2.6 Source characteristics and crustal structure for the TeraShake simulations. Depth variation depicts the isosurface of $V_s = 2.5$ km/s. Maximum slip (blue, <10.2 m) and maximum sliprate (red, <4.4 m/s) are projected along the TeraShake fault trace for the NW-SE and SE-NW1 rupture scenarios. CH = Chino Basin, LA = Los Angeles Basin, SBB = San Bernardino Basin, SBM = San Bernardino Mountains, SFV = San Fernando Valley, SGB = San Gabriel Basin, SGM = San Gabriel Mountains, and ST = Salton Trough. Other solid lines depict major freeways and the coastline. (Olsen *et al*, 2006)

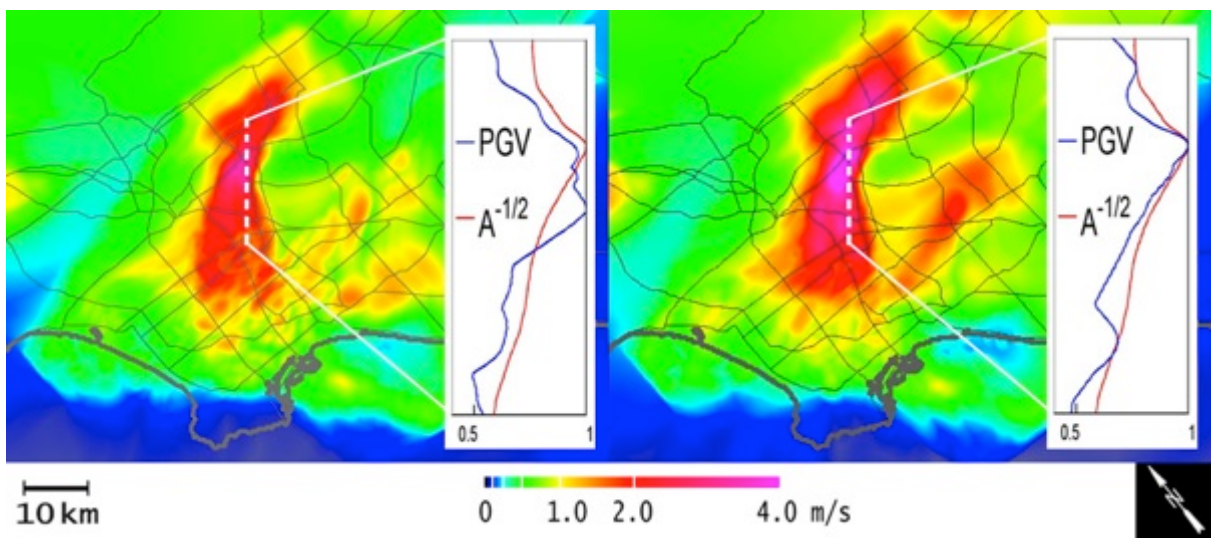


Figure 2.7 Maximum RMS PGV for (left) SE-NW1 and (right) SE-NW2 scenarios inside the black rectangle shown in Figure 1. The curves show the correlation of PGV (blue) and the reciprocal cross-sectional area (red) of the sediment channel between the Los Angeles and San Gabriel basins, measured as the area of the vertical cross-section striking N50°W that lies inside the 2 km/s S-wave speed isosurface. Both curves are normalized to their respective maxima along the dashed profile. Lines on the maps depict major freeways and the coastline. (Olsen *et al*, 2006)

U.S. Geological Survey studied the uniform California earthquake rupture forecast (2008). They found the results of 30-year probability of M6.7 event on San Andreas fault.

Table 2.1 30-year probability of M6.7 events on the Type-A faults, rounded to the nearest percent. (USGS, 2008)

Fault	WGCEP (2007) Mean [Min-Max]	WGCEP (2003) Mean [2.5% and 97.5%]	WGCEP (1995) Mean
Southern San Andreas	59% [22-94]		53%
Hayward-Rodgers Creek	31% [12-67]	27% [10-58]	
San Jacinto	31% [14-54]		61%
Northern San Andreas	21% [6-39]	23% [3-52]	
Elsinore	11% [5-25]		24%
Calaveras	7% [1-22]	11% [3-27]	
Garlock	6% [3-12]		

Table 2.1 summarizes the mean probabilities for M6.7 events on the principal strike-slip faults of California, which accommodate most of the motion between the North America and Pacific plates, and it compares our results with those of WGCEP 1995 for southern California and WGCEP 2003 for the Bay Area.

The most dangerous fault is the southern part of the San Andreas, which has a 59% probability of generating a M6.7 earthquake in the next 30 years. This compares with 21% for the northern San Andreas fault.

2.2 Theory

2.2.1 Ground Motion

Ground motion is the movement of the earth's surface from earthquakes or explosions. Ground motion is produced by waves that are generated by sudden slip on a fault or sudden pressure at the explosive source and travel through the earth and along its surface.

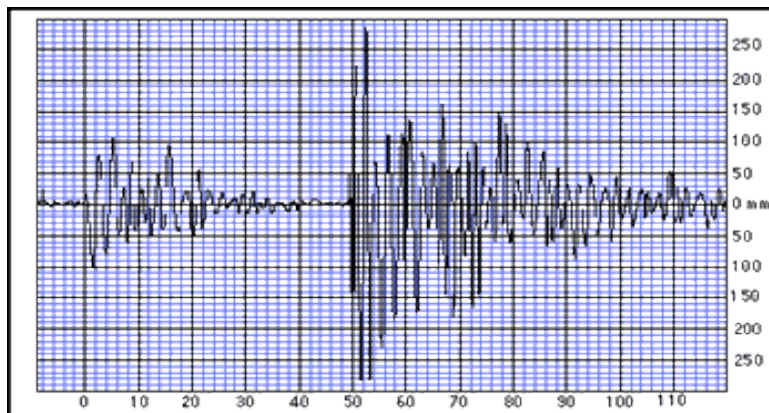


Figure 2.8 A recording of ground motion

< <http://earthquake.usgs.gov/learn/glossary/?term=ground%20motion>>

2.2.2 Green's Function

Green's function is a type of function used to solve inhomogeneous differential equations subject to specific initial conditions or boundary conditions. In term of seismology, Green's function is the response at the surface of inhomogeneous medium from the crosscorrelation of transmission responses using relationships derived from a two-way wavefield reciprocity theorem.

With seismic interferometry we can simulate seismic shot records at point A as if from a source at point B by crosscorrelating the seismic responses recorded at A and B. These responses can represent diffuse wavefields due to multiple scattering in deterministic or diffuse media or due to uncorrelated noise sources. We can also look at the recorded responses at A and B at the surface as due to active sources at the surface or due to passive sources in the subsurface. (Draganov, Wapenaar and Thorbecke, 2006)

$$GF(\vec{x}_{AB}, \omega) = u_A(\omega)u_B^*(\omega) \quad (2.5)$$

when u_A and u_B are the observed ground motion displacement recorded at A and B

2.2.3 Crosscorrelation

A simple thought experiment. Consider an example of a horizontally stratified (one-dimensional) acoustic medium, and for the moment let us imagine that it has only a single internal interface. Now, say horizontally planar pressure waves are emitted by two impulsive sources, one after the other, and that one source is above the interface and one below. Vibrations from the resulting propagating waves are recorded at two receivers which can be placed anywhere between the two sources.

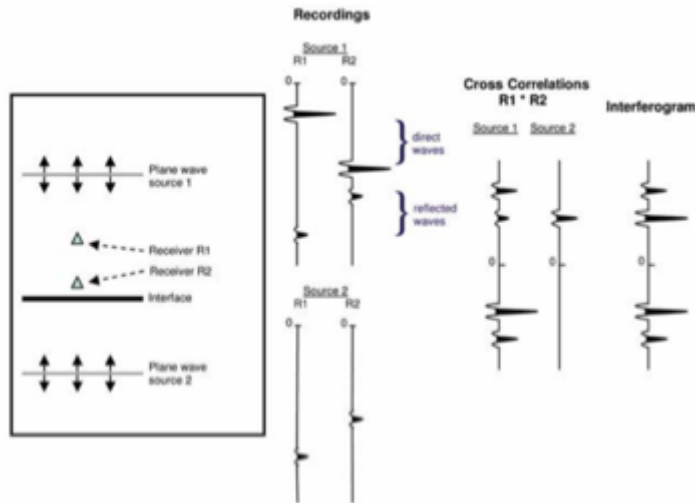


Figure 2.9 Interferometric construction of a virtual source. (left) One- dimensional acoustic medium consisting of single interface between two half-spaces, with two plane-wave sources and two receivers. (center) Traces recorded at each receiver for each source. (right) Crosscorrelations between pair of traces for source 1 and for source 2, and the sum of these crosscorrelations. At positive times, the final summed trace turns out to be the trace that would be recorded at one receiver if the other had been a source. (Curtis et al., 2006)

The recordings are shown in the center of the figure. At each receiver a direct and a reflected wave are recorded for source 1, whereas only one transmitted wave is recorded for source 2.

Seismic interferometry of these data involves only two simple steps: The two recorded signals from each source are crosscorrelated and the resulting crosscorrelograms are summed (stacked). The result, shown on the right of Figure 2.9., is surprising; for positive times it is the seismogram that would have been recorded at either receiver if the other receiver had in fact been a source, and at negative times it is the time reverse of this seismogram. In other words, by this simple, two-step operation we have constructed the seismic trace from a virtual source—a source that did not exist in our initial experiment, and a source that is imagined to be at the location of one of our receivers.

To generalize, this simple example placed no constraint on where the receivers were placed, provided they were between the sources. By moving either or both of them (or by using many distributed receivers from the start), it is therefore possible to construct the trace from an infinite number of virtual source and receiver pairs placed at any locations, by recording the signal from only two actual sources. What is more, provided one of the active sources is above the interface and receivers and the other is below, the location of the active sources is also arbitrary, and in order to carry out the process above we do not even need to know where these sources are.

Seismic interferometry steps, the fundamental steps of the operation are simple: crosscorrelation (we can understand this operation as detecting the traveltime difference of the recorded waves between the pair of receivers), then stacking (i.e., integration over all actual sources; a few details required to get the dynamics correct have been omitted for clarity). Yet, the technique is powerful and so far we have barely scratched the surface.

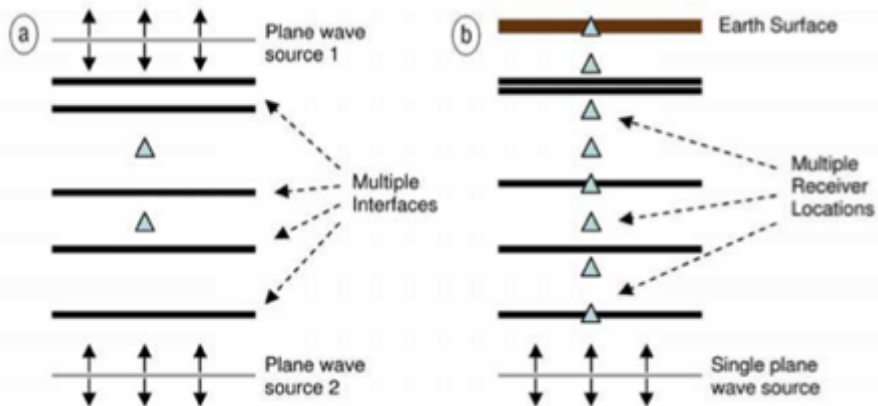


Figure 2.10 Alternative, more Earth-like models for which the process in Figure 2.9. works equally well. (left) Multiple layers with no free-surface still two sources required. (right) Multiple layers with a free-surface only one source required. The right plot also shows that any receiver locations can be used for the virtual source and receiver reconstruction. (Curtis et al., 2006)

The result above holds for any horizontally stratified medium, still using only two actual sources (Figure 2.10a.). The important criterion for the distribution of actual sources is that they completely surround the medium of interest (a portion of a one-dimensional medium is “surrounded” by two points, at the top and at the bottom). However, if any part of the boundary is a surface of total reflection (like the free surface of the Earth), it turns out that no source is required on that boundary. Hence, in 1D Earth-like models, only a single actual source is required to construct seismic traces between any source-receiver pair, including sources or receivers placed on the free surface (Figure 2.10b.). Now, consider a case in which a complex, multilayered medium is situated below the region of the model of interest (between the sources in Figure 2.10a.); this is probably realistic for the Earth. In that case, if source 2 is moved below this complex part of the medium, its contribution to the received signals becomes virtually zero due to transmission losses. In that case, the lower source in Figure 2.10a. can be neglected and again only a single active source is necessary to construct the inter- receiver seismic traces.

The above example also shows us how to make sense of noise and cudas (the long, multiply reflected tails of data observed on seismic traces). It turns out that impulsive sources on the boundary can be replaced by uncorrelated noise sources that emit continually and simultaneously. Any pair of extensive noise records from any two receivers

can then be crosscorrelated and, remarkably, the result will be approximately the same as above: The crosscorrelation will approximate the impulse response (the measured wavefield at one location if an impulsive source is placed at the location of the other) on the right of Figure 2.9., convolved with a source time function that is the autocorrelation of the noise.

The term interferometry generally refers to the study of interference phenomena between pairs of signals in order to obtain information from the differences between them. Seismic interferometry simply refers to the study of interference of seismic-related signals. The principal mathematical operation used to study this interference is crosscorrelation of pairs of signals, but one could equivalently consider convolution as the principal operation because crosscorrelation is simply convolution with the reverse of one of the two signals. The signals themselves may come from background-propagating waves or reverberations in the Earth, from earthquakes, from active artificial seismic sources, from laboratory sources, or from waveforms modeled on a computer. (Curtis et al., 2006)

2.2.4 Seismic Interferometry

Seismic interferometry involves the crosscorrelation of responses at different receivers to obtain the Green's function between these receivers. For the simple situation of an impulsive plane wave propagating along the x -axis, the crosscorrelation of the responses at two receivers along the x -axis gives the Green's function of the direct wave between these receivers, in case at x_A and x_B .

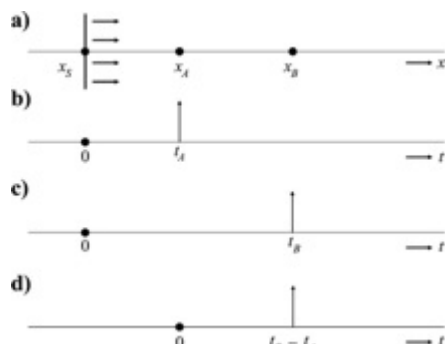


Figure 2.11 A 1D example of direct-wave interferometry. (a) A plane wave traveling rightward along the x -axis, emitted by an impulsive source at $x=x_S$ and $t=0$. (b) The response observed by a receiver at x_A . This is the Green's function $G(x_A,x_S,t)$. (c) As in (b) but for a receiver at x_B . (d) Crosscorrelation of the responses at x_A and x_B . This is interpreted as the response of a source at x_A , observed at x_B , i.e., $G(x_B,x_A,t)$. (Wapenaar et al., 2010)

Looking at Figure 2.11a, it appears that the raypaths associated with $G(x_A, x_S, t)$ and $G(x_B, x_S, t)$ have the path from x_S to x_A in common. The traveltime along this common path cancels in the crosscorrelation process, leaving the traveltime along the remaining path from x_A to x_B , i.e., $t_B - t_A = (x_B - x_A)/c$. Hence, the crosscorrelation of the responses in Figure 2.11b and c is an impulse at $t_B - t_A$ (see Figure 2.11d). This impulse can be interpreted as the response of a source at x_A observed by a receiver at x_B , i.e., the Green's function $G(x_B, x_A, t)$. The crosscorrelation of impulse response at x_A and x_B is $G(x_A, x_S, t)^*G(x_B, x_S, -t)$.

$$G(x_B, x_A, t) = G(x_B, x_S, t) * G(x_A, x_S, -t) \quad (2.6)$$

Note that the source is not necessarily an impulse. If the source function is defined by some wavelet $s(t)$, then the responses at x_A and x_B can be written as $u(x_A, x_S, t) = G(x_A, x_S, t)^*s(t)$ and $u(x_B, x_S, t) = G(x_B, x_S, t)^*s(t)$, respectively. Let $S_s(t)$ be the autocorrelation of the wavelet, i.e., $S_s(t) = s(t)^*s(-t)$. Then the crosscorrelation of $u(x_A, x_S, t)$ and $u(x_B, x_S, t)$ gives the right-hand side of equation 1, convolved with $S_s(t)$. This is equal to the left-hand side of equation above, convolved with $S_s(t)$. Therefore, the equation below shows the Green's function in case of wavelet $s(t)$ is source. (Wapenaar *et al.*, 2010)

$$G(x_B, x_A, t) * S_s(t) = u(x_B, x_S, t) * u(x_A, x_S, -t) \quad (2.7)$$

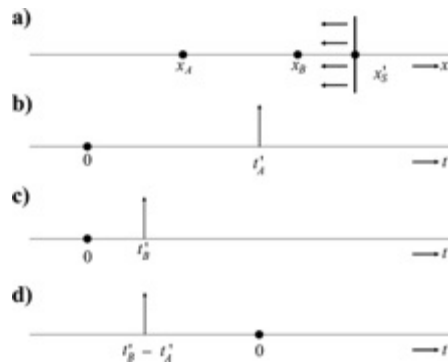


Figure 2.12 As in Figure 2.11 but this time for a leftward-traveling impulsive plane wave.

The crosscorrelation in (d) is interpreted as the time-reversed Green's function $G(x_B, x_A, -t)$.

(Wapenaar *et al.*, 2010)

2.2.5 Coda-wave

Coda waves are considered the result of scattering processes caused by heterogeneities acting on seismic waves. P and S waves play a particularly important role in this interaction. The process introduces an attenuation which, added to the intrinsic absorption, gives the observed apparent attenuation. Therefore, coda waves constitute a thumbprint left by the heterogeneities on the seismograms. Coda waves offer decisive information about the mechanism of how scattering and attenuation take place. (Herraiz and Espinosa, 1987)

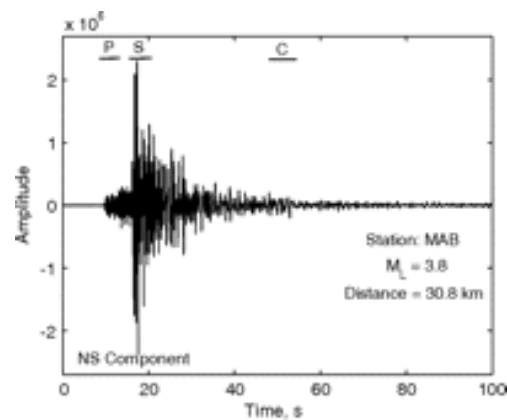


Figure 2.13 Seismogram shows body and coda wave (Kayal, 2011)

Coda waves are sensitive to changes in the subsurface because the strong scattering that generates these waves causes them to repeatedly sample a limited region of space. Coda wave interferometry is a technique that exploits this sensitivity to estimate slight changes in the medium from a comparison of the coda waves before and after the perturbation. For spatially localized changes in the velocity, or for changes in the source location, the travel-time perturbation may be different for different scattering paths. The coda waves that arrive within a certain time window are therefore subject to a distribution of travel-time perturbations. (Snieder, 2006)

2.2.6 Fast Fourier Transform

Fast Fourier Transform (FFT) is a faster version of Discrete Fourier Transform (DFT). The DFT is extremely important in the area of frequency (spectrum) analysis

because it takes a discrete signal in the time domain and transforms that signal into its discrete frequency domain representation.

<<http://www.ele.uri.edu/~hansenj/projects/ele436/fft.pdf>>

$$f(t) = \frac{1}{2\pi} \int_{-\infty}^{\infty} F(\omega) e^{i\omega t} d\omega \quad (2.8)$$

2.2.7 Seismic Noise

Seismic noise exists everywhere on the Earth surface. It mainly consists in surface waves, which are the elastic waves produced by the constructive interference of the P and S waves in the layers near the surface. Seismic noise is mostly produced by wind and sea waves. Also industries and vehicle traffic locally generate seismic noise, although essentially at high frequencies (some Hz), which are quickly attenuated.

<<http://www.tromino.it/application.htm>>

CHAPTER III

METHODOLOGY

Methodology

Follow the steps below to achieve the Green's function.

1. Review and study previous works that are related to this project from published papers.
 - 1.1 Review the fundamental information about southern California especially the fault and earthquake system.
 - 1.2 Study the literature about the principle and methodology of extracting Green's function and ground motion.
2. Download the earthquake data of the magnitude 7.2 Sierra El Mayor earthquake of Sunday April 4th 2010, occurred in northern Baja California, which approximately 40 miles south of the Mexico-USA border.

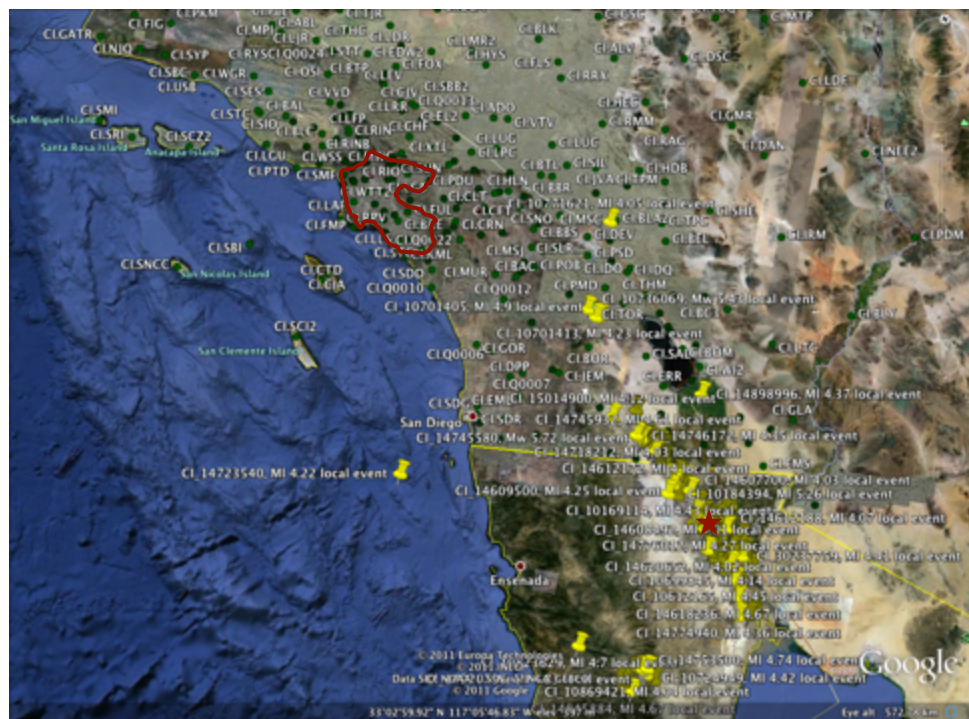


Figure 3.1 Locations of Los Angeles sedimentary basin (red curve), seismic broadband stations (green circle) and earthquake (yellow pins). The epicenter of M 7.2 Sierra El Mayor earthquake represents by red star. <<http://www.google.com/earth/download/ge/agree.html>>

- 2.1 Download the recorded seismic wave of magnitude 7.2 Sierra El Mayor earthquake of Sunday April 4th 2010 from Southern California Earthquake Data Center.
- 2.2 Check the quality of that data and deleted bad files.
- 2.3 Study the characteristic of the earthquake that includes the characteristic of P-wave, S-wave, Coda-wave, amplitude and arrival time of each wave.
3. Remove the instrument response because the observation ground displacement is the result of the convolution of seismic source function, seismic propagation function or Green's function and instrument recording function or instrument response.
- The observation ground motion displacement $u(t)$
- $$u(t) = s(t) * g(t) * i(t) \quad (2.9)$$
- when $u(t)$: An observed ground motion displacement
 $s(t)$: Seismic source function
 $g(t)$: Seismic propagation function or Green's function that depend on earth structure
 $i(t)$: Instrument recording function or instrument response
- Thus, deconvolving the instrument response is a common step to convert the recorded trace into meaningful ground motion.
- 3.1 Study the methodology to remove the instrument response
- 3.2 Write the C++ script to do bandpass filtering. In this project we filtered the frequency of all seismic data with low-pass filter, 0.01-0.05 Hz, and high pass filter, 15-20 Hz.
4. Pick time window of Coda-wave. Coda wave is scattered wave that follow the passing of the first wave generated by an earthquake and the beginning of the coda was originally assigned to the point where the amplitude decay starts to be exponential.
- 4.1 Study the literatures about the characteristic of coda-wave.

4.2 Study and check the characteristic of our seismic data after removed instrument response.

4.3 Study the relationship between time arrival of coda-wave of our seismic data and other wave.

4.4 Write the MATLAB script to pick time window of coda-wave and applied to all seismic data.

After studied the characteristic of coda-wave, we found that time arrival of coda-wave is equal to two time of average time arrival of surface wave. So we have to find the average time arrival of surface wave. In case of this area, surface wave velocity is about 2-5 km/s. If we divide the distance from source to each station location (every seismic data that downloaded from each station will contain the distance between source and that station) by 2 km/s and 5 km/s, we will know the range of time arrive of surface wave. According to high amplitude of surface wave, we can find the exactly time arrival of surface wave by finding the highest amplitude in that range of time arrival of surface wave. Then we will know the time arrival of coda-wave because coda-wave time arrival is equal to two time of time arrival of surface wave. Because we have a lot of seismic data that means we have a lot of coda-wave. There are two ways to pick time window of coda-wave, first is pick by hand and other is write the program script to pick time window automatically. According to a lot of data we have, it's impossible that we can cut by hand. From the relationship of coda-wave and surface wave, we can write to MATLAB script to pick all time window of coda-wave automatically. And the length of coda-wave we used in this project is 800 s.

4.5 Check the quality of all coda-waves after picked time window by using the MATLAB script we wrote.

5. Apply fast fourier transform (FFT) to transform data from time domain to frequency domain. In seismometry, it is often useful to represent transient time domain signals by an equivalent function in the frequency domain so

all results from the previous step need to be applied Fast Fourier Transform (FFT) to work in frequency domain by using the relationship between time and frequency of signal the shows below.

$$f(t) = \frac{1}{2\pi} \int_{-\infty}^{\infty} F(\omega) e^{i\omega t} d\omega \quad (2.10)$$

6. Apply coherency or crosscorrelation function, which is a measurement of similarity of two waveforms to retrieve the Green's function in frequency domain. Then stack data to distribute the source coverage. The equation below shows the retrieved Green's function between station A and B.

$$G_{AB}(\omega) = \frac{\langle u_A(\omega) u_B^*(\omega) \rangle}{\{|u_A(\omega)|\} \{|u_B(\omega)|\}} \quad (2.11)$$

This step we used the same script that used to applied coherency to retrieve seismic noise Green's function.

7. Compare the extracted Green's function with Green's functions determined from the seismic noise.
8. Estimate ground motion by applying transfer function to simulate ground motion map of southern California in case of M7+ earthquake occur along the San Andreas fault.

$$TF_{AB}(\omega) = \frac{\langle u_A(\omega) u_B^*(\omega) \rangle}{\{|u_B(\omega)|\}^2} \quad (2.12)$$

9. Discussion and conclusion
10. Make report and present the entire project.

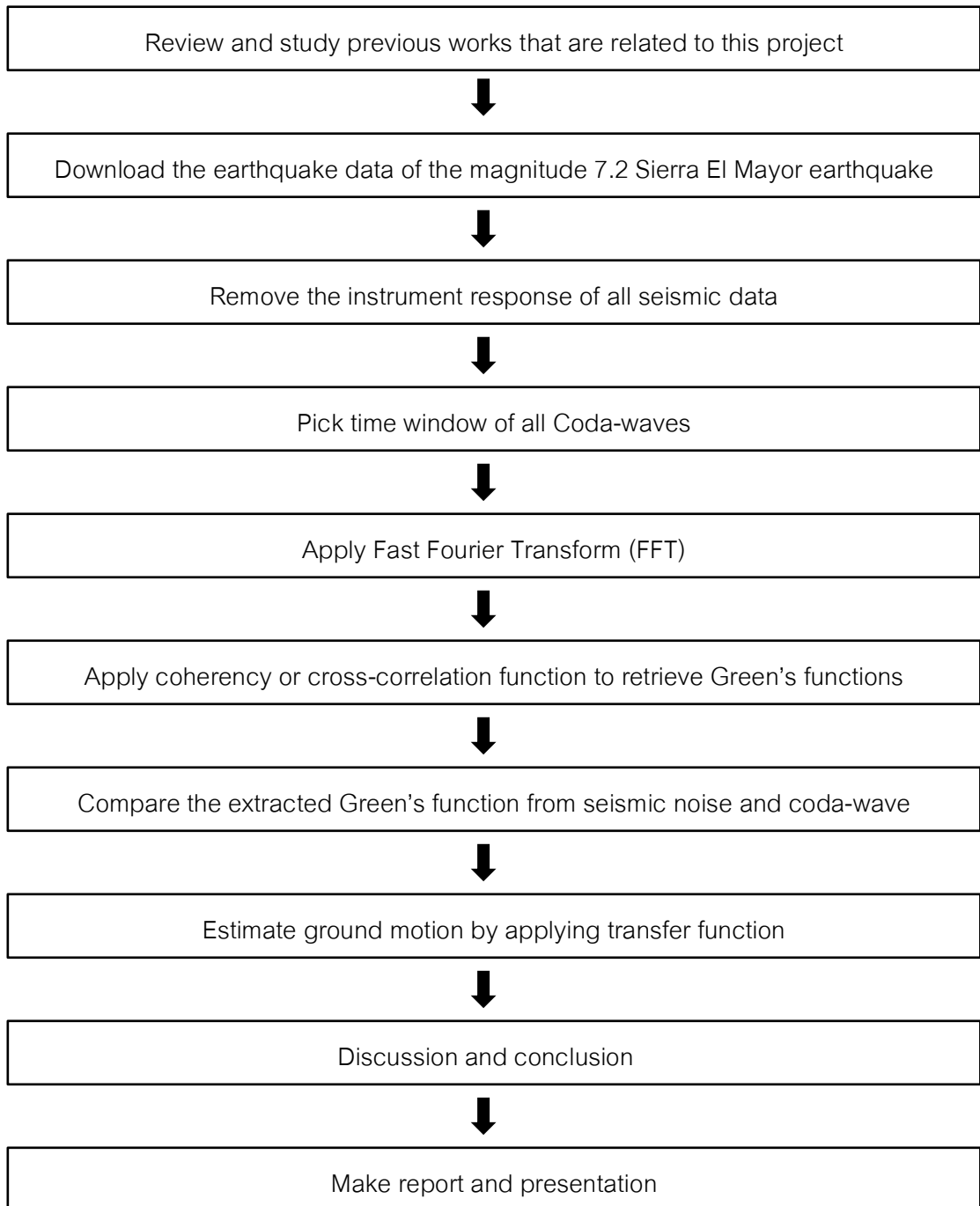


Figure 3.2 Methodology flowchart

CHAPTER IV

RESULT AND INTERPRETATION

Result and Interpretation

After we applied the methodology step by step, the results from each step were interpreted as below.

1. Downloaded seismic data

According to the earthquake occurred in Baja California, Mexico. The seismic waves were recorded at about 150 seismic stations around southern California. These are examples of seismic data of the magnitude 7.2 Sierra El Mayor earthquake of Sunday April 4th 2010.

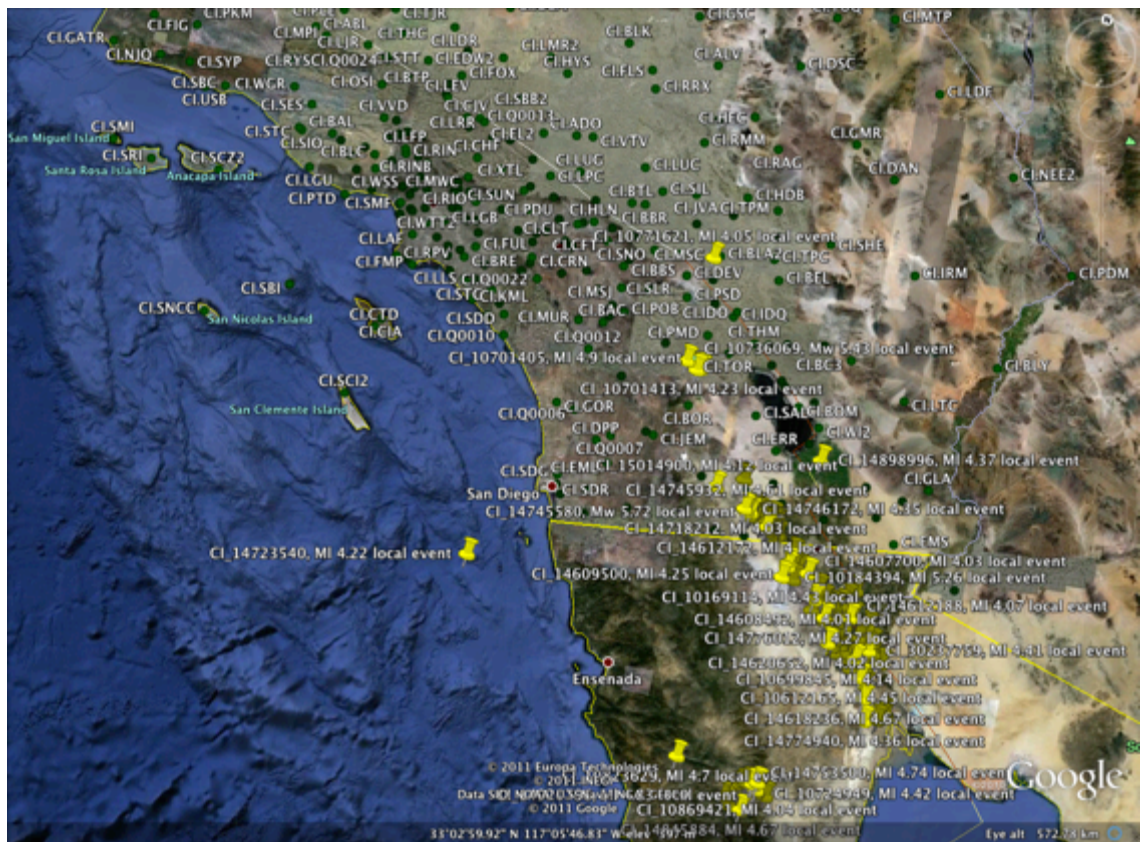


Figure 4.1 Locations of seismic broadband stations (green circle) around southern California that recorded seismic wave of M7.2 El Mayor earthquake.

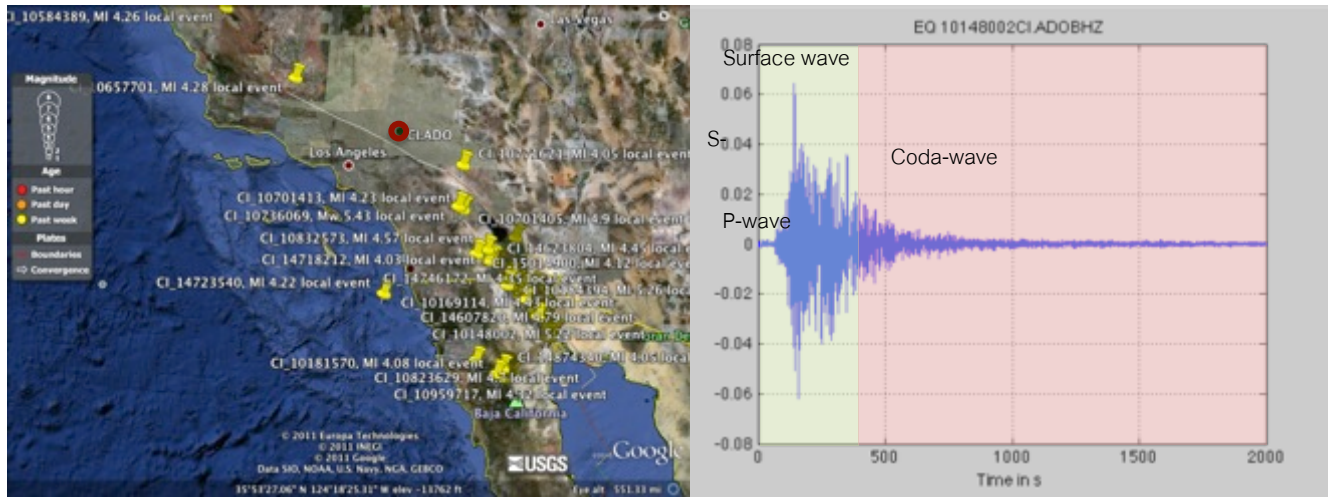


Figure 4.2 Locations of seismic broadband station CI_ADO represents by red circle and earthquakes represent by yellow pins (left). [<http://www.google.com/earth/download/ge/agree.html>](http://www.google.com/earth/download/ge/agree.html)
The characteristic of seismic data that recorded by this station (right).

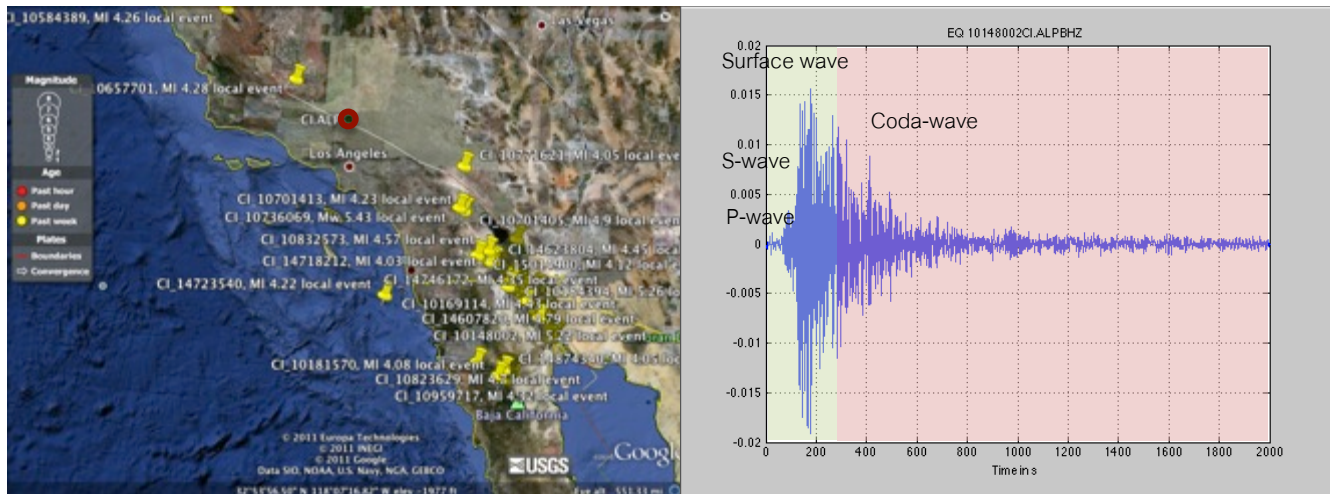


Figure 4.3 Locations of seismic broadband station CI_ALP represents by red circle and earthquakes represent by yellow pins (left). [<http://www.google.com/earth/download/ge/agree.html>](http://www.google.com/earth/download/ge/agree.html)
The characteristic of seismic data that recorded by this station (right).

2. Remove instrument response and pick time window of coda-wave

These are examples of seismic data after remove instrument response and pick time window of coda-wave and use 800 seconds as a length of coda-wave.

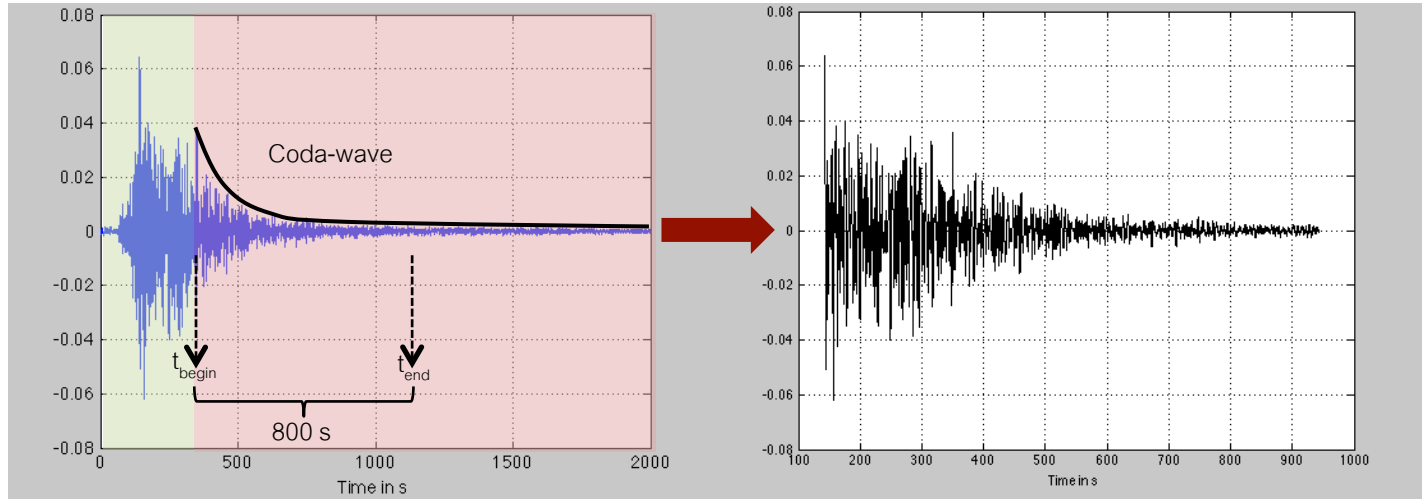


Figure 4.4 The seismic data of M 7.2 Sierra El Mayor earthquake recorded by seismic broadband station CI_ADO before pick time window of Coda-wave (left) and after picked time window of Coda-wave (right).

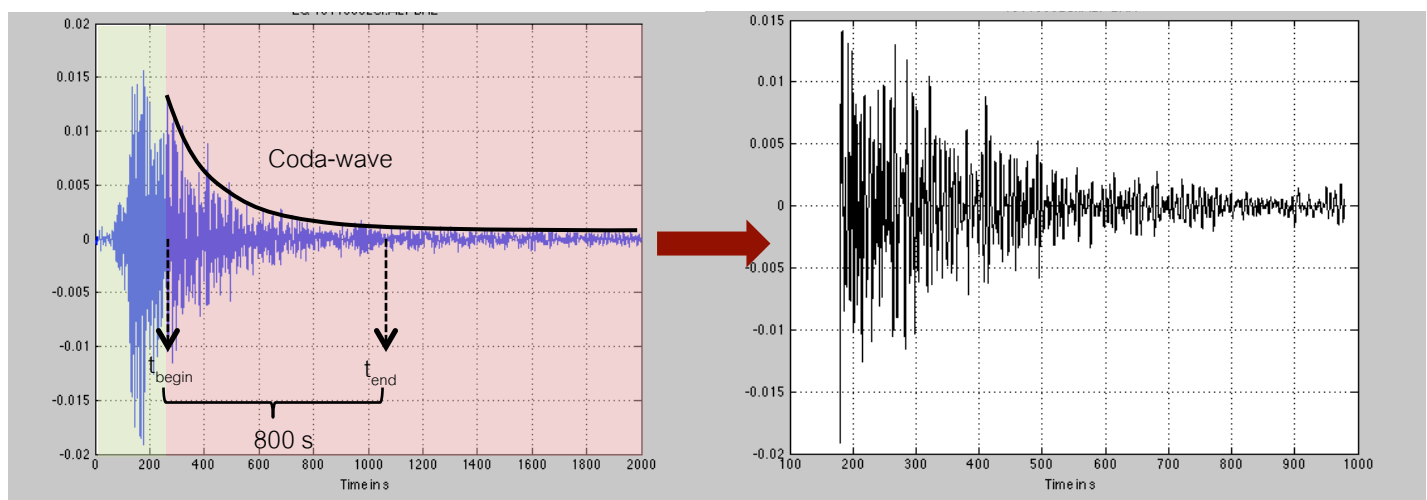


Figure 4.5 The seismic data of M 7.2 Sierra El Mayor earthquake recorded by seismic broadband station CI_ALP before pick time window of Coda-wave (left) and after picked time window of Coda-wave (right).

3. After applied FFT and coherency or crosscorrelation to retrieve coda-wave Green's function. The results of Green's function between each seismic broadband station pair can be divided into 2 groups. The coda-wave Green's functions show by

3.1 Symmetric Green's function

This type of Green's function show the symmetry between position and negative part of Green's function that mean forces are distributed and came from all direction around seismic broadband station pair.

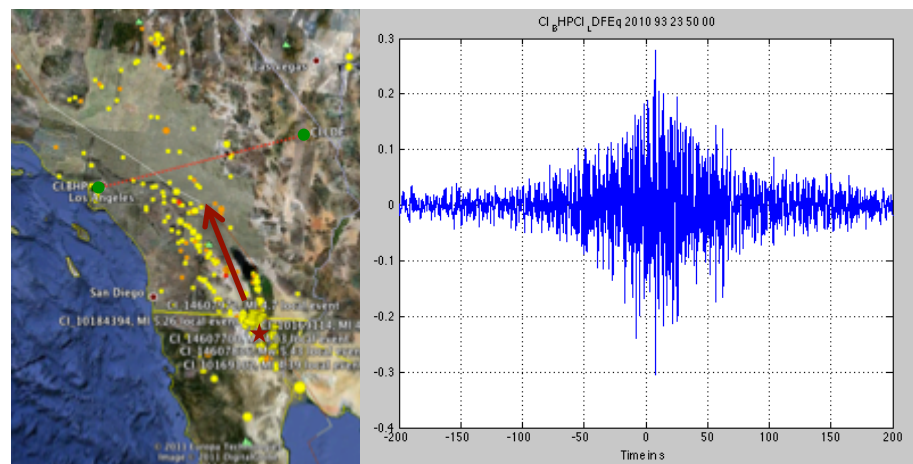


Figure 4.6 Locations of seismic station CI_LDF (source) and CI_BHP (receiver) represent by green circles and red star shows the location of earthquake (left).

<<http://www.google.com/earth/download/ge/agree.html>>

The characteristic of Green's function between these two stations (right).

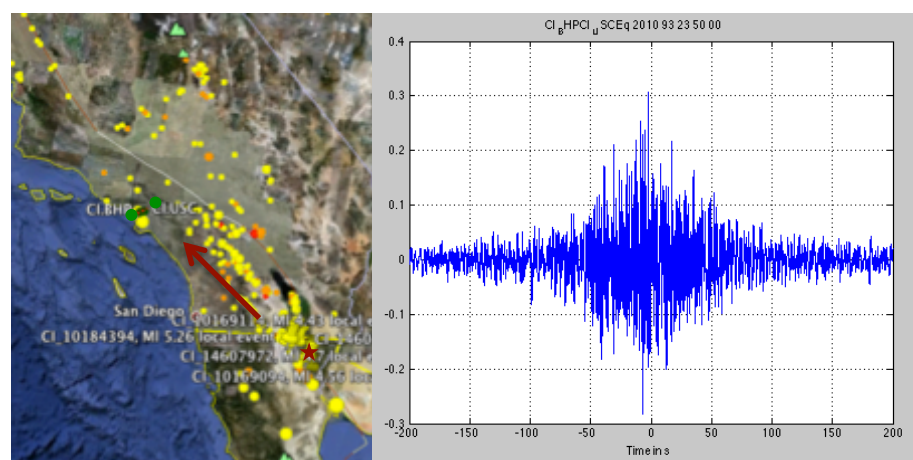


Figure 4.7 Locations of seismic station CI_USC (source) and CI_BHP (receiver) represent by green circles and red star shows the location of earthquake (left).

<<http://www.google.com/earth/download/ge/agree.html>>

The characteristic of Green's function between these two stations (right).

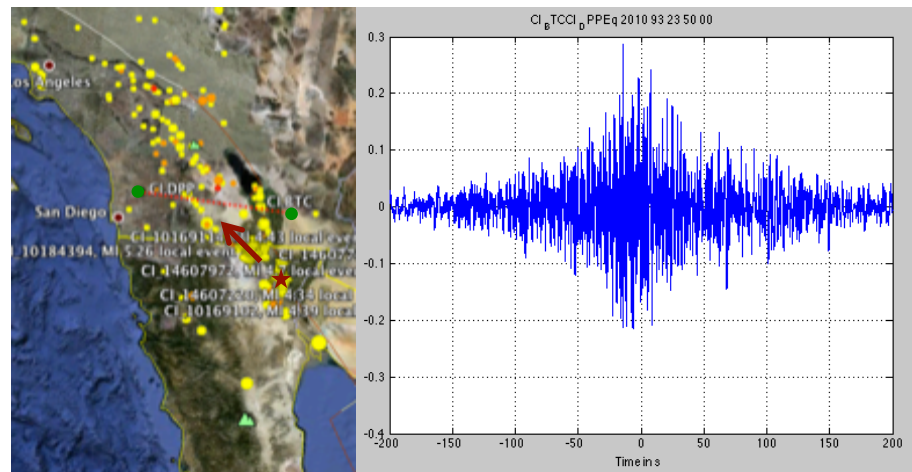


Figure 4.8 Locations of seismic station CI_DPP (source) and CI_BTC (receiver) represent by green circles and red star shows the location of earthquake (left).
[<http://www.google.com/earth/download/ge/agree.html>](http://www.google.com/earth/download/ge/agree.html)
The characteristic of Green's function between these two stations (right).

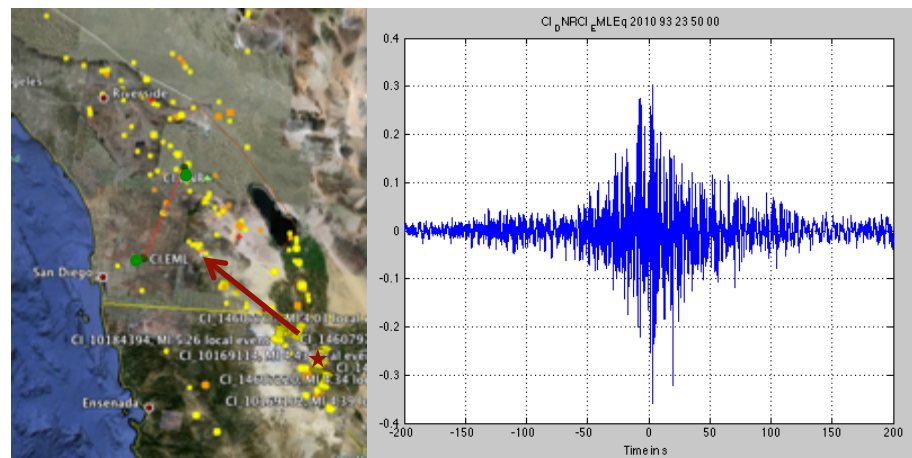


Figure 4.9 Locations of seismic station CI_EML (source) and CI_DNR (receiver) represent by green circles and red star shows the location of earthquake (left).
[<http://www.google.com/earth/download/ge/agree.html>](http://www.google.com/earth/download/ge/agree.html)
The characteristic of Green's function between these two stations (right).

From 4 examples of Symmetric Green's function above, we found that most of Symmetric Green's functions come from the station pairs that perpendicular to the source. Symmetrical shape of Green's function represents the equal source from all direction around seismic station. If seismic station pair is perpendicular to the source, most of energy will not come from one station (or one direction) of station pair so when we applied seismic interferometry

technic we found Symmetric Green's function. According to the theory, Symmetric Green's function is like an ideal case that can use to estimate more accuracy ground motion.

We observe many of the locations of broadband station that represent the Symmetric Green's function. In the map below, the black lines show all seismic station pairs that we retrieved the Symmetric Green's function and the seismograms show the example of comparison of coda-wave Symmetric Green's function (blue) and seismic noise Symmetric Green's function (red).

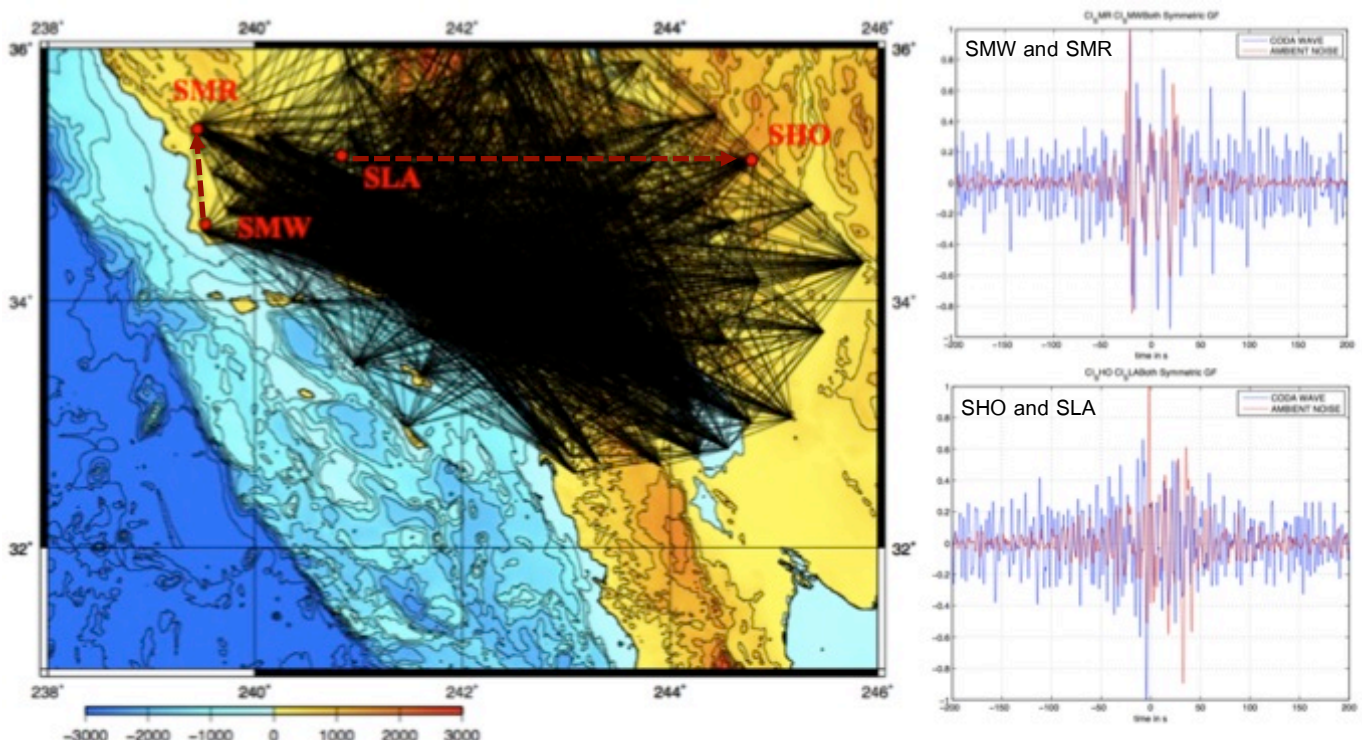


Figure 4.10 Map shows location of broadband station that represents the Symmetric Green's function (left). Comparison of coda-wave Green's function (blue) and seismic noise Green's function (red) computed from the station SMW and SMR (upper right) SLA and SHO (lower right).

3.2 Anti-symmetric Green's function

This type is the opposite from the first one because the characteristic of Green's function shows asymmetry between positive and negative part of Green's function that mean forces mostly came from one direction.

3.2.1 Anti-symmetric causal Green's function

The Green's function calculates from crosscorrelation of each seismic broadband station pair that will use one station as a source and other

one as a receiver. If the source located on the same direction of force, in this case force is cause by earthquake in Baja California, which located on the SE of Los Angeles sedimentary basin, the Green's function will represent most of energy in the positive part. This type of Green's function calls "Anti-symmetric causal Green's function".

These are the example of Anti-symmetric causal Green's function.

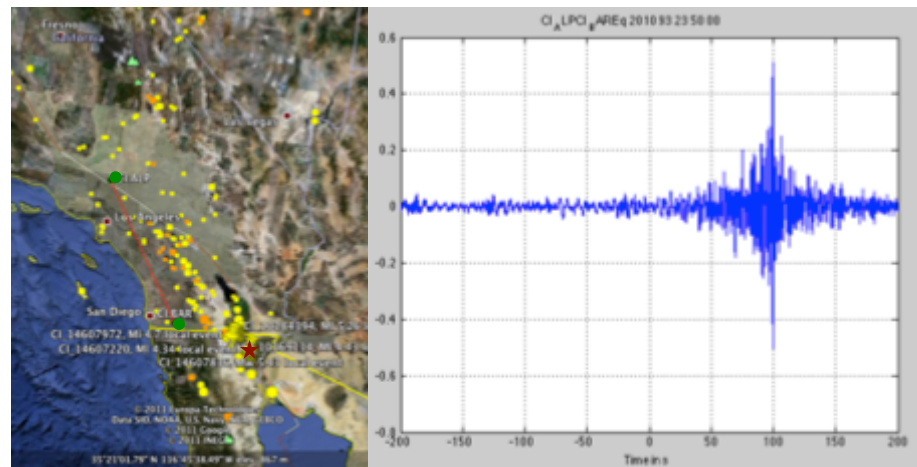


Figure 4.11 Locations of seismic station CI_BAR (source) and CI_ALP (receiver) represent by green circles and red star shows the location of earthquake (left).

<<http://www.google.com/earth/download/ge/agree.html>>

The characteristic of Green's function between these two stations (right).

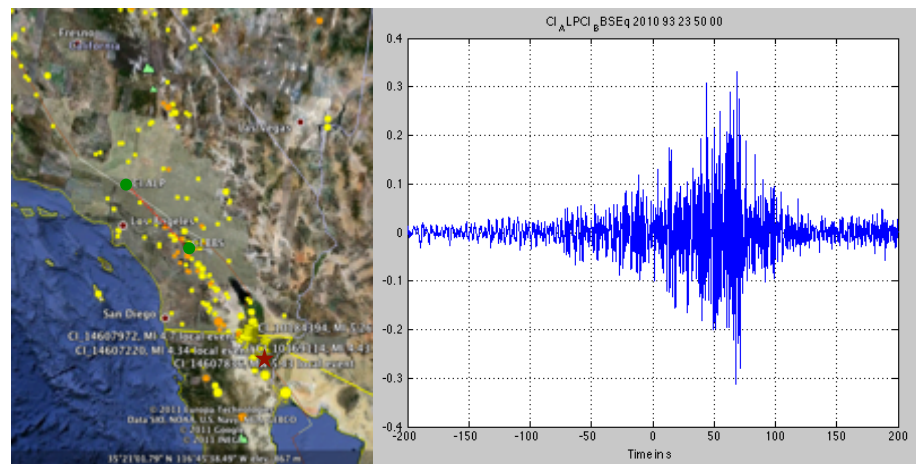


Figure 4.12 Locations of seismic station CI_BBS (source) and CI_ALP (receiver) represent by green circles and red star shows the location of earthquake (left).

<<http://www.google.com/earth/download/ge/agree.html>>

The characteristic of Green's function between these two stations (right).

We observe many of the locations of broadband station that represent the Anti-symmetric causal Green's function. In the map below, the black lines show all seismic station pairs that we retrieved the Anti-symmetric causal Green's function and the seismograms show the example of comparison of coda-wave Anti-symmetric causal Green's function (blue) and seismic noise Anti-symmetric causal Green's function (red).

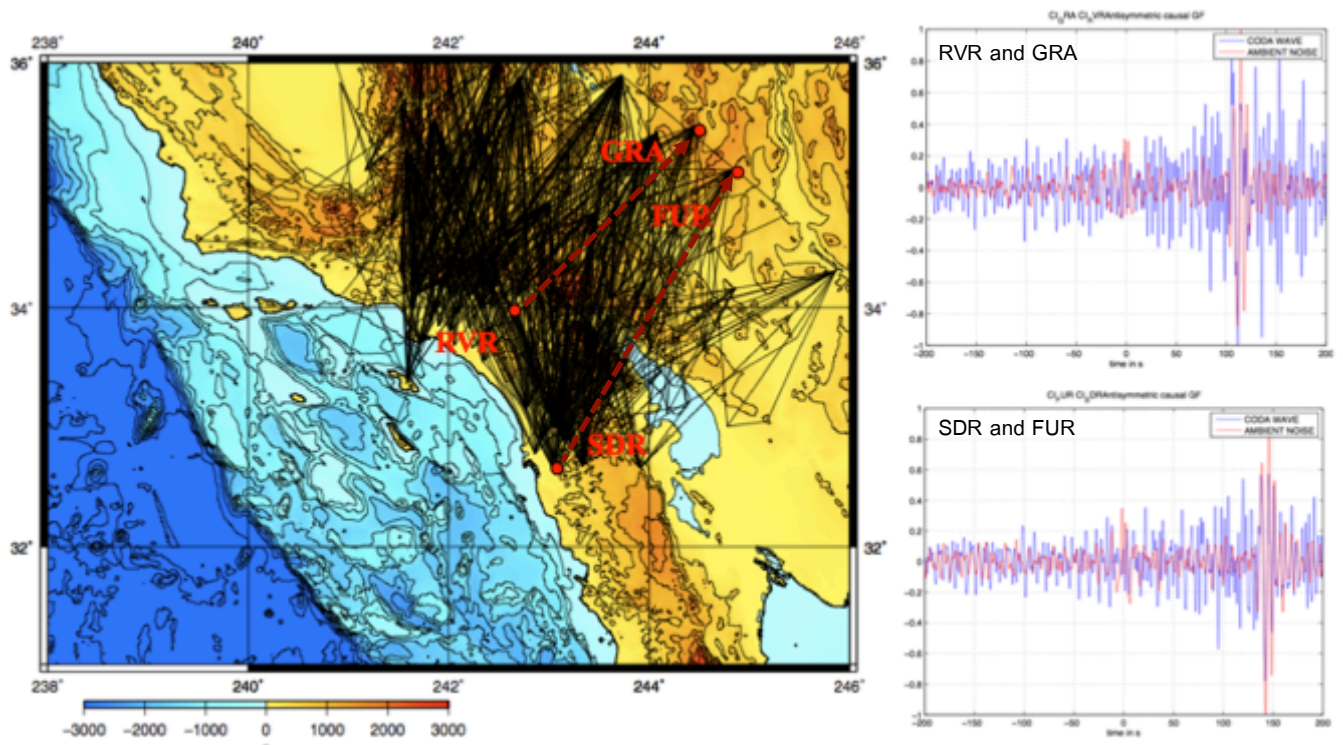


Figure 4.13 Map shows location of broadband station that represents the Anti-symmetric causal Green's function (left). Comparison of coda-wave Green's function (blue) and seismic noise Green's function (red) computed from the station RVR and GRA (upper right) SDR and FUR (lower right).

3.2.2 Anti-symmetric anti-causal Green's function

On the other hand, if the source located on the opposite direction of force, the Green's function will represent most of energy in the negative part. This type of Green's function calls "Anti-symmetric anti-causal Green's function".

These are the example of Anti-symmetric anti-causal Green's function.

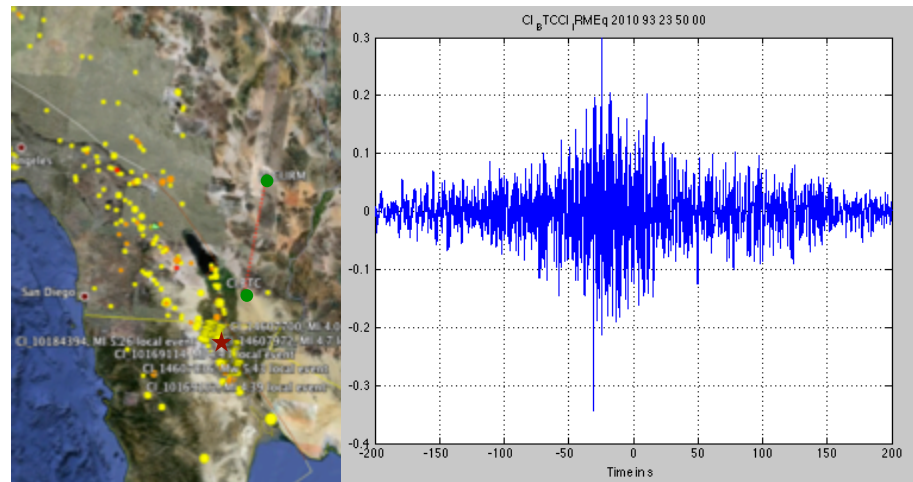


Figure 4.14 Locations of seismic station CI_IRM (source) and CI_BTC (receiver) represent by green circles and red star shows the location of earthquake (left).

[<http://www.google.com/earth/download/ge/agree.html>](http://www.google.com/earth/download/ge/agree.html)

The characteristic of Green's function between these two stations (right).

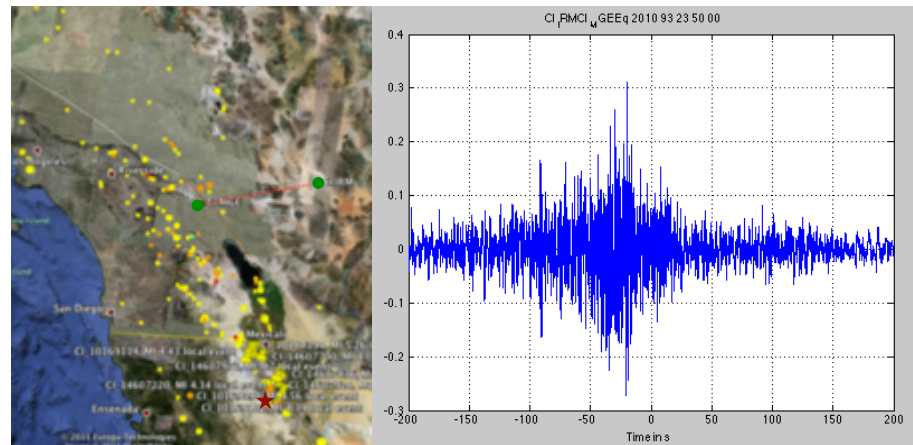


Figure 4.15 Locations of seismic station CI_MGE (source) and CI_IRM (receiver) represent by green circles and red star shows the location of earthquake (left).

[<http://www.google.com/earth/download/ge/agree.html>](http://www.google.com/earth/download/ge/agree.html)

The characteristic of Green's function between these two stations (right).

We observe many of the locations of broadband station that represent the Anti-symmetric anti-causal Green's function. In the map below, the black lines show all seismic station pairs that we retrieved the Anti-symmetric anti-causal Green's function and the seismograms show the example of comparison of coda-wave Anti-symmetric anti-causal

Green's function (blue) and seismic noise Anti-symmetric anti-causal Green's function (red).

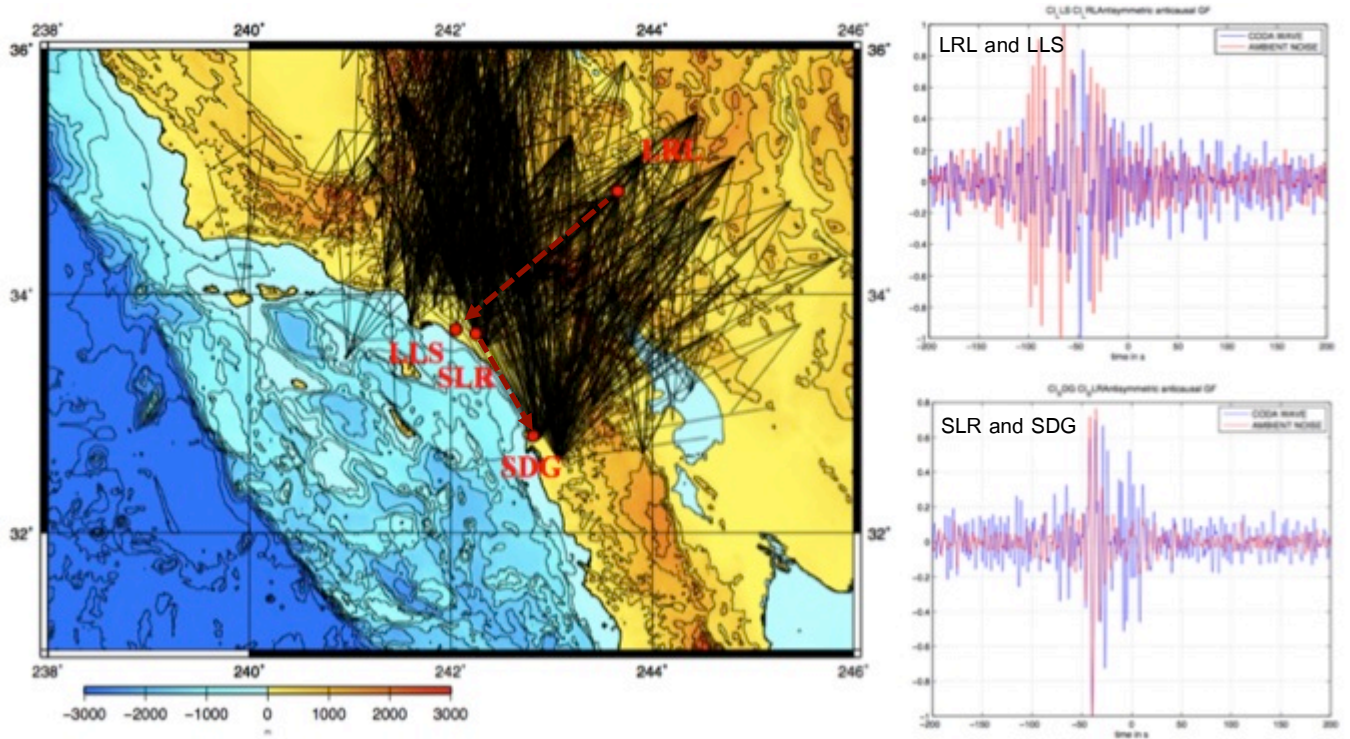


Figure 4.16 Map shows location of broadband station that represents the Anti-symmetric anti-causal Green's function (left). Comparison of coda-wave Green's function (blue) and seismic noise Green's function (red) computed from the station LRL and LLS (upper right) SLR and SDG (lower right).

According to the coda-wave Green's function and seismic noise Green's function, we found that in some specific station pair the coda-wave Green's function represent the opposite direction of energy from seismic noise Green's function. This type of result we call the complementary Green's function. The map below shows the locations of the complementary Green's function. From this type of results, the combination of coda-wave Green's function and seismic noise Green's function will help us to retrieve more symmetric Green's function which means we will get more accurate Green's function.

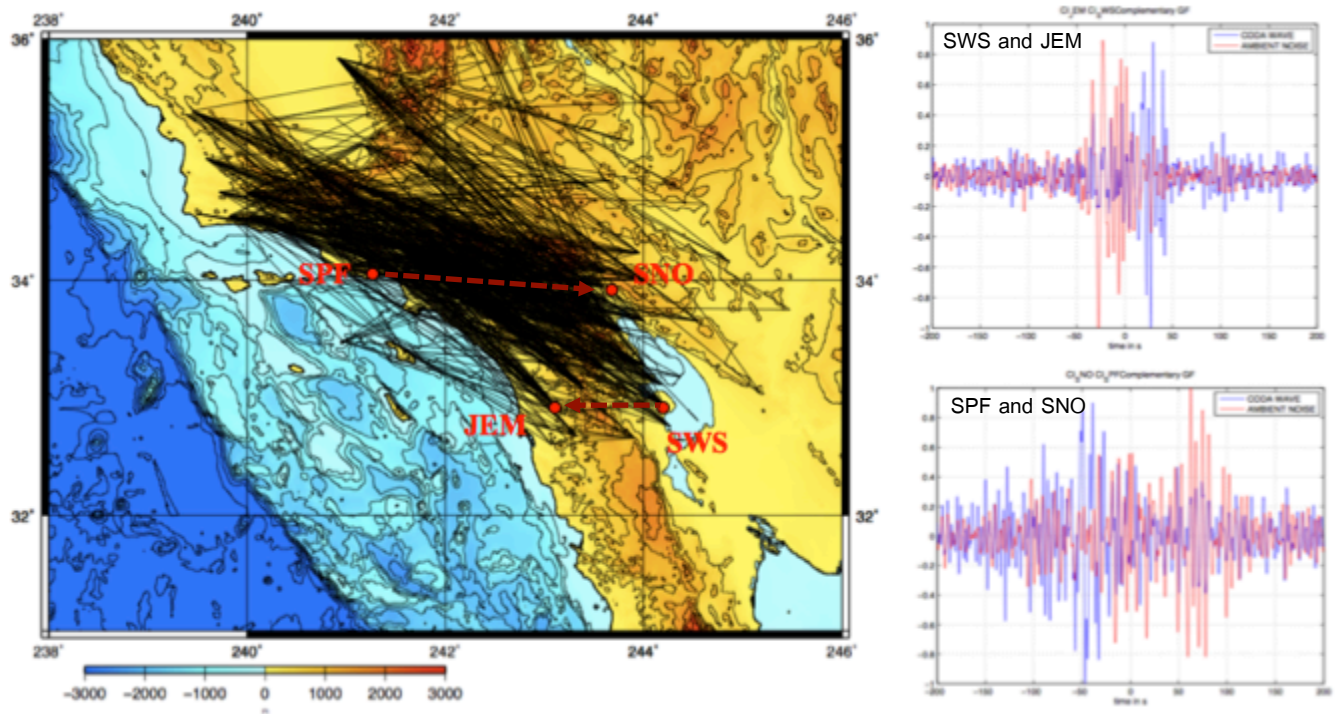


Figure 4.17 Map shows location of broadband station that represents the complementary Green's function (left). Comparison of coda-wave Green's function (blue) and seismic noise Green's function (red) computed from the station SWS and JEM (upper right) SPF and SNO (lower right).

From all of the results above, we have the network of coda-wave Green's functions which represent the response of the earth due to the propagation of earthquake or seismic wave around southern California so we can use this Green's function to predict ground motion in this area.

In case we used station BFS as a seismic source and seismic wave propagate from here to other station. We observed the coda-wave Green's function that can be divide into groups as shows in the map below.

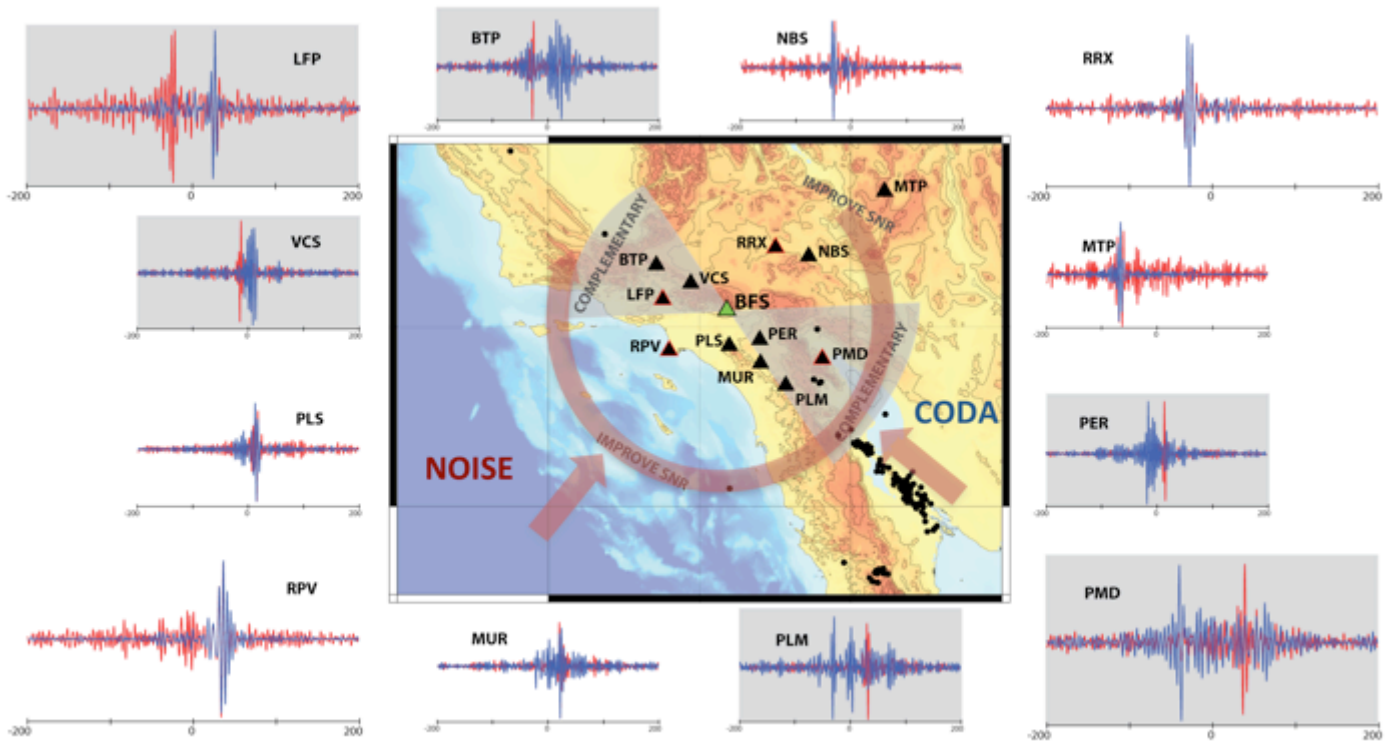


Figure 4.18 Map shows location of broadband station that represent the example of Green's function comparison of coda-wave Green's function (blue) and seismic noise Green's function (red) in case the source is at station BFS.

4. Applied transfer function to estimate ground motion. According the 30-year probability of M6.7 event on San Andreas fault, we found that there is 59% that this area, southern California, will be face the M7+ due to the earthquake along the southern San Andreas fault. Then we estimate the ground motion in case of seismic source is at station located on the southern San Andreas fault.

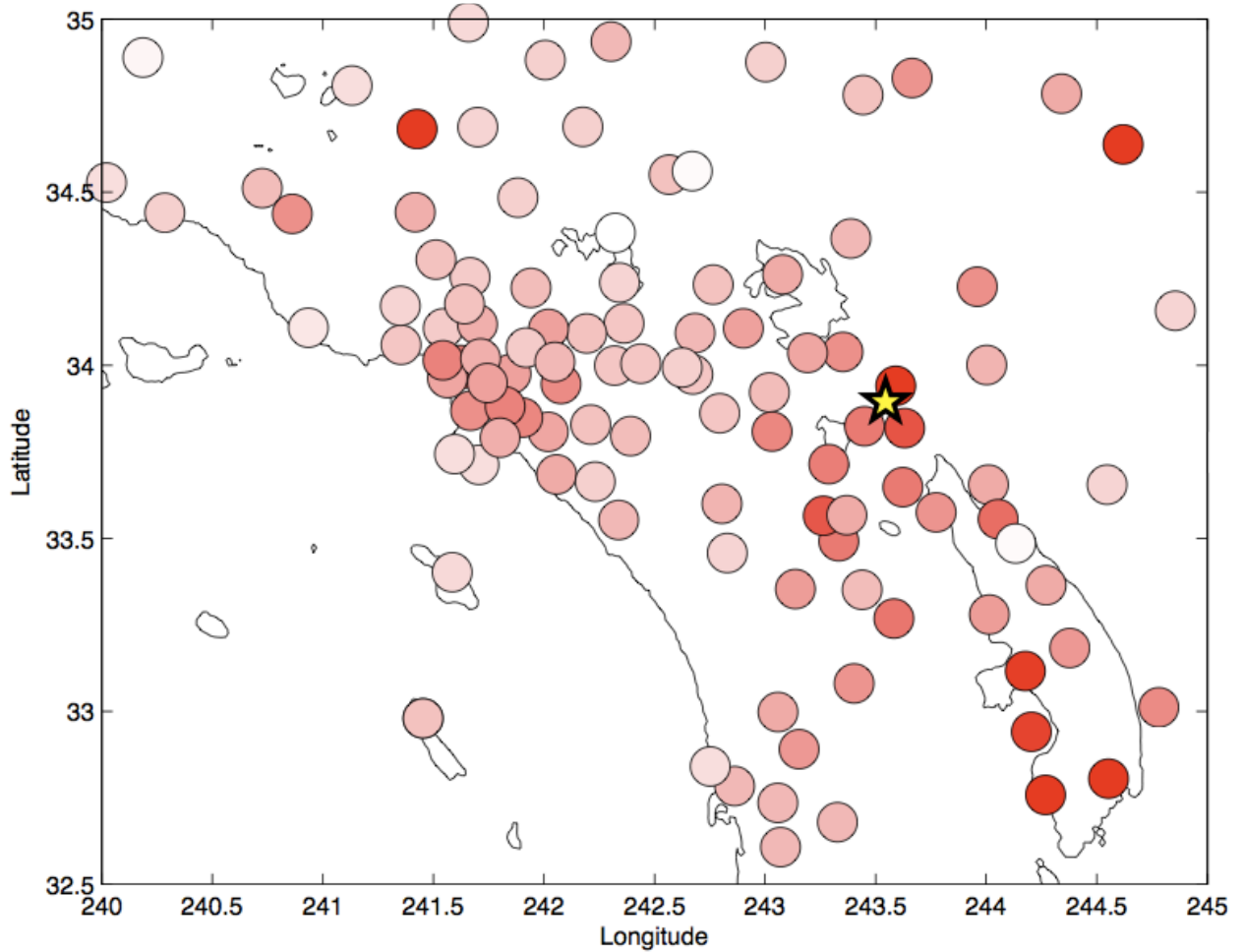


Figure 4.19 Hazard map or ground motion map represents the level of ground shaking (more red means more shaking level) in case of M7+ occur along the southern San Andreas fault (star).

CHAPTER V

DISCUSSION AND CONCLUSION

5.1 Discussion and Conclusion

In this study, we used coda-wave interferometry of the M7.2 El Mayor-Cucapah aftershock to extract the Green's functions for stations along the southern San Andreas fault, and compared the results with Green's functions determined from the seismic noise. By stacking the crosscorrelation function of coda-wave, we found that the Green's function can be extracted from coda-wave interferometry technic and we observed that in some cases coda-wave Green's function are better than seismic noise Green's function because it has higher signal to noise ratio than seismic noise Green's function that implied more accurate Green's function.

We observed both Symmetric and Anti-symmetric Green's function by using coda-wave interferometry technique. For the Anti-symmetric part, we found that amplitudes at positive and negative times are not equal and represent the causal and anti-causal parts of the Green's function. We explained this observation by anisotropy of the diffuse field with most of energy coming from the south. This is a reflection of the fact that the distribution of earthquakes is not isotropic around the station. Furthermore, the combination of coda-wave Green's function and seismic noise Green's function would greatly enhance the accuracy of the retrieved Green's function.

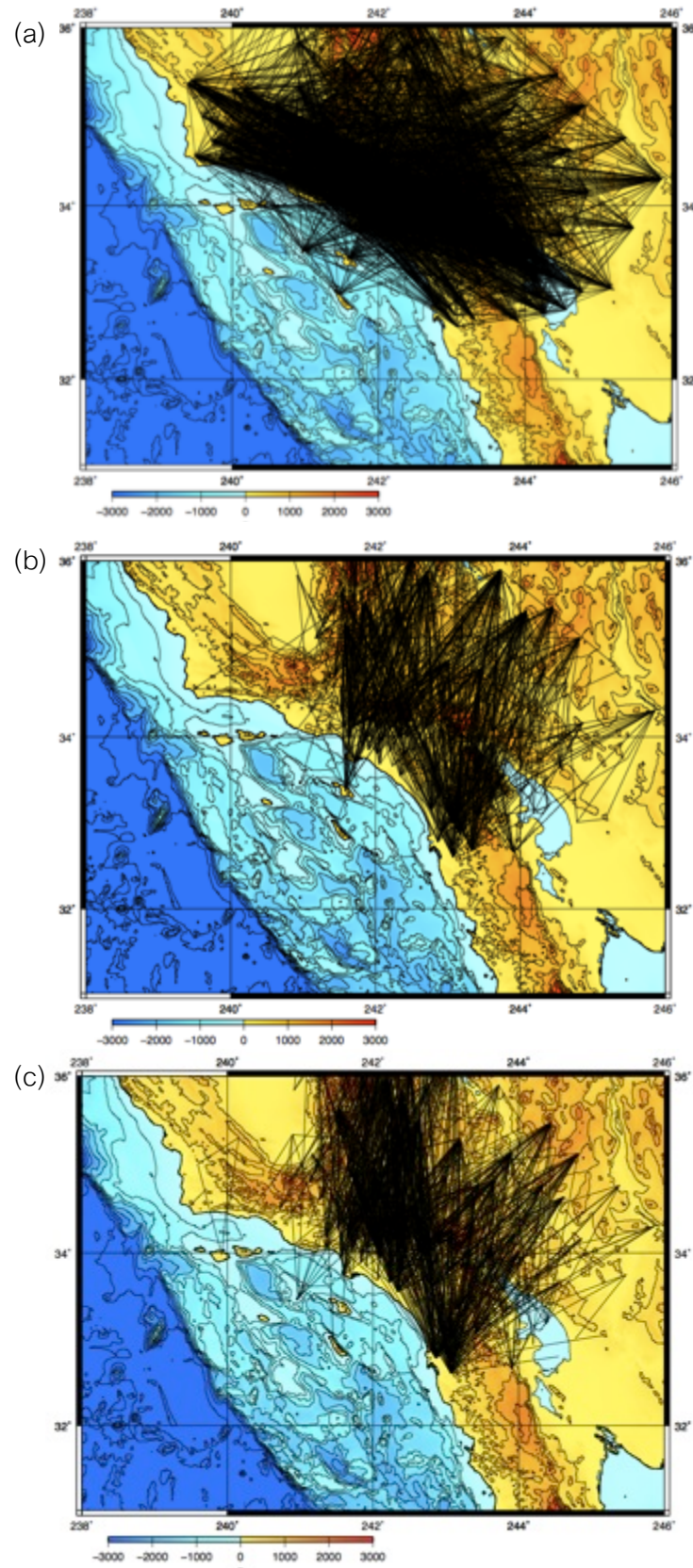


Figure 5.1 Map shows location of broadband station that represents the Symmetric Green's function
 (a), Anti-symmetric causal Green's function (b) and Anti-symmetric anti-causal Green's function.

Finally, obtained coda-wave Green's function can be used to predict ground motion in Los Angeles sedimentary basin as a response to M7+ earthquake on the San Andreas Fault.

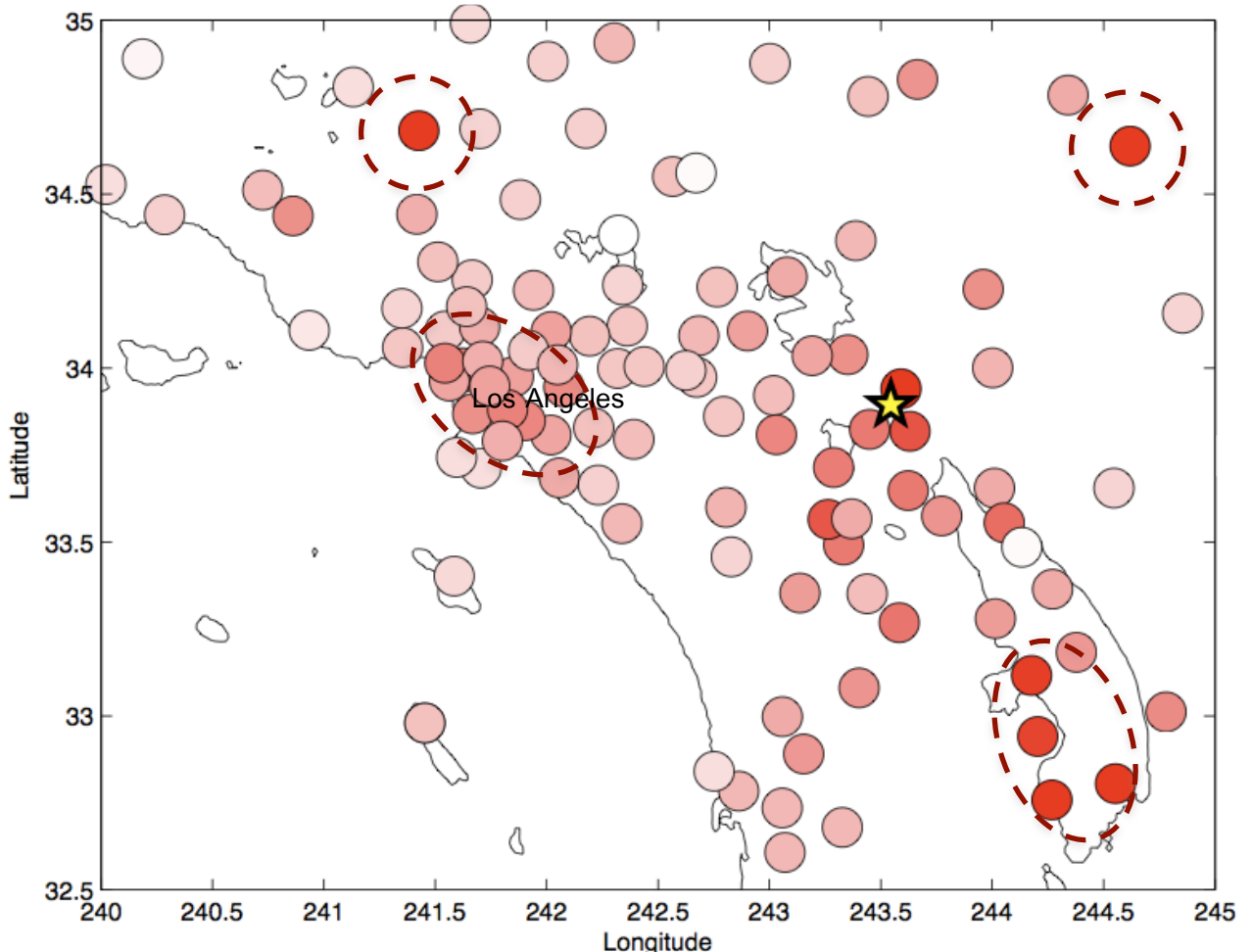


Figure 5.2 Hazard map or ground motion map represents the level of ground shacking (more red means more shacking level) that is not follow the geometric spreading.

According to the ground motion map above, in case of M7+ earthquake occur at the location of star, along the San Andreas fault, we observed that the level of ground shaking is decrease away from the source due to the attenuation of seismic wave when it propagate through the earth. But in some area shows by dash line ellipse, the shaking level is not follow the geometric spreading because we found the amplification of seismic wave that represents by the increasing of red color. One ellipse is the location of Los Angeles sedimentary basin and because of the soft sediment in this basin, the amplitude

of seismic wave was amplified. Moreover, in the area of Los Angeles sedimentary basin, the amplification is different. We observed more amplification at the center of basin than the basin rim. However, there are three more dash line ellipse that show the amplification areas in southern California that is interesting and need more studied to conclude that why the seismic wave is amplified in that area. The lower dash ellipse is possible that the high shaking level is because those stations are located on the segment of southern San Andreas fault.

5.2 Recommendation

Although we have a lot of seismic data, we need to check the quality of the raw data and also the result from each step as much as possible.

REFERENCES

- Campillo M. and Paul A., 2003. Long-Range Correlations in the Diffuse Seismic Coda. Science. Vol.299, 547-549.
- Curtis A. et al., 2006. Seismic interferometry – turning noise into signal. The leading edge. Vol.25, No.9, 1082-1092.
- Draganov D., Wapenaar K. and Thorbecke J., 2006. Green's Function Representations for Seismic Interferometry. Geophysics. Vol.71, No.4, S133-S146.
- Herraiz M. and Espinosa A.F., 1987. Coda waves: A review. Pure and Applied Geophysics PAGEOPH. Vol. 125, No. 4, 499-577.
- Kayal J.R., 2011. Frequency-Dependent Attenuation of Body and Coda Waves in the Andaman Sea Basin. Bulletin of the Seismological Society of America. Vol. 101, No. 1, 109-125.
- Lobkis O. I. and Weaver R. L., 2001. On the emergence of the Green's function in the correlations of a diffuse field. Acoustical Society of America. Vol.110, No. 6, 3011-3017.
- Lobkis O. I. and Weaver R. L., 2002. On the emergence of the Green's function in the correlations of a diffuse field: pulse-echo using thermal phonons. Ultrasonics. Vol.40, 435-439.
- Olsen K. B. et al., 2006. Strong shaking in Los Angeles expected from southern San Andreas earthquake. Geophysical Research Letters. Vol. 33, L07305.
- Prieto G. A. and Beroza G. C., 2008. Earthquake ground motion prediction using the ambient seismic field. Geophysical Research Letters. Vol. 35, L14304.
- Shapiro N. M. and Campillo M., 2004. Emergence of boardband Rayleigh wave from correlations of the ambient seismic noise. Geophysical Research Letters. Vol. 31, L07614.
- Shapiro N. M. et al., 2005. High-resolution surface wave tomography from ambient seismic noise. Science. Vol. 307, 1615-1618.
- Snieder R., 2006. The Theory of Coda Wave Interferometry. Pure and Applied Geophysics. Vol. 163, 455-473.

- U.S. Geological Survey., 2008. The Uniform California Earthquake Rupture Forecast, Version2 (UCERF2), 1-104.
- Wapenaar K. *et al.*, 2010. Tutorial on seismic interferometry: Part1-Basic principle and applications. Geophysics. Vol. 75, No. 5, 195-209.
- Zhang J.P. *et al.*, 2010. Resolving p-wave travel-time anomalies using seismic array observations of oceanic storms. Earth Planet Science Letters. Vol. 292, 419-427.
- GNC Science. (2011) Fault rupture, 1987 Edgecumbe earthquake. Available at <http://www.teara.govt.nz/en/earthquakes/2/3> (Accessed 20 March 2012).
- Google. (2011) Google Earth (Version 6) [Computer program]. Available at <http://www.google.com/earth/download/ge/agree.html> (Accessed 27 August 2011).
- National Institute of Advance Industrial Science and Technology (AIST). Available at http://www.aist.go.jp/index_en.html (Accessed 20 March 2012).
- Skoola. (2010) How Earthquakes And Tsunami Work. Available at http://skoola.com/read_news.php?id=190 (Accessed 10 March 2012).
- State University of New York. (2009) Disaster Resilience. Available at <http://mceer.buffalo.edu/research/resilience> (Accessed 10 March 2012).
- The State of California. (2010) California Geological Survey – 2010 State Geologic Map of California. Available at http://www.conservation.ca.gov/cgs/cgs_history/Pages/2010_geologicmap.aspx (Accessed 20 March 2012).
- Tromino. (2011) Seismic noise and its applications. Available at <http://www.tromino.it/application.htm> (Accessed 10 September 2011).
- University of Rhode Island Department of Electrical and Computer Engineering. (2011) FFT Tutorial. Available at <http://www.ele.uri.edu/~hansenj/projects/ele436/fft.pdf> (Accessed 10 September 2011).
- U.S. Geological Survey. (2006) Geologic History of the San Andreas Fault System. Available at http://geomaps.wr.usgs.gov/archive/socal/geology/geologic_history/san_andreas_history.html (Accessed 27 August 2011).

- U.S. Geological Survey. (2009) Earthquake Glossary – amplification. Available at <http://earthquake.usgs.gov/learn/glossary/?term=amplification> (Accessed 27 August 2011).
- U.S. Geological Survey. (2009) Earthquake Glossary – ground motion. Available at <http://earthquake.usgs.gov/learn/glossary/?term=ground%20motion> (Accessed 27 August 2011).
- U.S. Geological Survey. (2010) M7.2 – Baja California, Mexico. Available at <http://earthquake.usgs.gov/earthquakes/dyfi/events/ci/14607652/us/index.html> (Accessed 20 March 2012)

APPENDICES

APPENDIX A The C++ Script to Remove Instrument Response

```

#!/bin/tcsh
#
set dir = '/Users/penprapawutthijuk/RAW_DATA/EQ_DATA'
set dir2 = $dir/RESP_FILES
cd $dir
foreach Eq (1* 3*)
    cd $dir2
    foreach St (CI*)
        echo $Eq, $St
        foreach Ch (BHE BHN BHZ)
            set f = $dir/$Eq/$Eq.$St.$Ch.sac
            set d = $dir2/$St/${St}_$Ch.pz

sac << EOF
r $f
rtrend
rmean
rtrend
rmean
rtrend
rmean
transfer from polezero subtype $d to none freqlimits 0.01 0.05 15 20
rtrend
rmean
mkdir /Users/penprapawutthijuk/RAW_DATA_rminstr/$Eq
write dir /Users/penprapawutthijuk/RAW_DATA_rminstr/$Eq $Eq.$St.$Ch.sac
exit
EOF

                end
            end
            cd $dir
        end

#mv -r directory/* .

```

APPENDIX B The MATLAB Script to Pick Time Window of Coda-wave

```
% script 1 Prepare for pick Coda wave automatic

% initialisation
clear all
close all
clc
addpath '~/lib_mat/'

% directories where data are (change Eq id of dir and dirout)
dir = '~/EQ_DATA';
dirout = '~/EQ_DATA_CODA_new';

listEq = importdata('~/list_eq_ae_ndata.dat');

listSt = importdata ('~/ list_st_ae_ndata.dat');

L_coda = 800; %in seconds
t = (0:0.025:250);

set (gca,'Fontsize',14);
[a,b]=butter(2,[1 5]/20);

% script pick Coda wave automatic for BHN.sac file

for i2=1:length(listEq)

    for i1=1:length(listSt)

        fname = [char(dir) '/' char(int2str(listEq(i2))) '/'
char(int2str(listEq(i2))) '.' char(listSt(i1)) '.BHN.sac']

        if exist(char(fname), 'file') == 2

            z=readsac(char(fname));
            toto=filtfilt(a,b,z.trace);
            figure(1)
            plot(t(1:min([length(z.trace)
length(t]))),z.trace(1:min([length(t) length(z.trace)))));

            grid on;
            z.dist
            z.b

            % plot(t(1:min([length(z.trace)
length(t]))),toto(1:min([length(t) length(z.trace)])), 'r');
            % grid on;
            xlabel ('Time in s')
            title ([char(int2str(listEq(i2))) ' ' char(listSt(i1)) ' '
BHN']);
            hold on
            pause

            % pick coda (pick time of begin and end of coda length)
```

```

%
%      2x surface wave arrival (vs ~3.5 km/s)
%      t1(1)=3*z.dist/3.5;
%      t1(2)=t1(1)+L_coda; % keep at least 800s of signal.
%      if (z.e-t1(1)+z.b))>=L_coda

%
%      remove bad data
%      t1(1)=z.dist/5;
%      t2(1)=z.dist/2;

[ia,ib]=max(abs(z.trace(floor(t1(1)/z.dalta):floor(t2(1)/z.delta
))));

%
ib*z.delta;

t1(1)=t1(1)+ib*z.delat;
t1(2)=t1(1)+L_coda;

i=((floor(t1(1)/z.delta)):floor((t1(2)/z.delta)));

%
[ia,ib]=max(abs(z.trace(1:floor(t1(1)/z.delta))));

ik = find(abs(z.trace(i))<ia);

if length(ik) < floor(L_coda/z.delta)
    disp('bad station!')
    disp(z.dist)
    continue
end

dt=z.delta;
z2=zeros(floor(2000/dt),1);

z2(i)=z.trace(i);
t2=t(i);

figure(2)
plot(t(i),z2(i));
grid on;

disp([int2str(floor(t1(2)/dt)-floor(t1(1)/dt))])

plot(t(floor(t1(1)/dt):floor(t1(2)/dt)),z2(floor(t1(1)/dt):floor
(t1(2)/dt)), 'k');

grid on;

xlabel ('Time in s')
title ([char(int2str(listEq(i2))) ' ' char(listSt(i1)) ' BHN'])
pause

z.b = 0;%t1(1)+z.b;
z.e = 1200;
z.npts = floor((1200/dt);
z.trace = z2;

%
% write in new directory

```

```

    % create new dir
    dir2 = [char(dirout) '/' char(int2str(listEq(i2))) ]
    system(['mkdir ' char(dir2)])
    fcuname = [char(dir2) '/' char(int2str(listEq(i2))) '.'
char(listSt(i1)) '.BHN.sac'];

    writesac(z,char(fcuname));

    disp(['Eq =' char(int2str(i2)) ])
    disp(['St =' char(int2str(i1)) ])
    end
    close all
    end
end

% script pick Coda wave automatic for BHZ.sac file

for i2=1:length(listEq)

    for i1=1:length(listSt)

        fname = [char(dir1) '/' char(int2str(listEq(i2))) '/'
char(int2str(listEq(i2))) '.' char(listSt(i1)) '.BHZ.sac']

        if exist(char(fname), 'file') == 2

            z = readsac(char(fname));
            toto = filtfilt(a, b, z.trace);
            figure(1)
            plot(t(1:min([length(z.trace)
length(t)))), z.trace(1:min([length(t) length(z.trace)))));

            grid on;
            z.dist
            z.b

            % plot(t(1:min([length(z.trace)
length(t)))), toto(1:min([length(t) length(z.trace)])), 'r');
            % grid on;
            xlabel ('Time in s')
            title ([char(int2str(listEq(i2))) ' ' char(listSt(i1)) ' '
BHZ']);
            hold on
            pause

            % pick coda (pick time of begin and end of coda length)

            % 2x surface wave arrival (vs ~3.5 km/s)
            % t1(1)=3*z.dist/3.5;
            % t1(2)=t1(1)+L_coda; % keep at least 800s of signal.
            % if (z.e-t1(1)+z.b)>=L_coda

            % remove bad data
            t1(1)=z.dist/5;
            t2(1)=z.dist/2;

```

```

    [ia,ib]=max(abs(z.trace(floor(t1(1)/z.dalta):floor(t2(1)/z.delta
))));

%      ib*z.delta;

t1(1)=t1(1)+ib*z.delat;
t1(2)=t1(1)+L_coda;

i=((floor(t1(1)/z.delta)):floor((t1(2)/z.delta)));

%      [ia,ib]=max(abs(z.trace(1:floor(t1(1)/z.delta))));

ik = find(abs(z.trace(i))<ia);

if length(ik) < floor(L_coda/z.delta)
    disp('bad station!')
    disp(z.dist)
    continue
end

dt=z.delta;
z2=zeros(floor(2000/dt),1);

z2(i)=z.trace(i);
t2=t(i);

figure(2)
plot(t(i),z2(i));
grid on;

disp([int2str(floor(t1(2)/dt)-floor(t1(1)/dt))])

plot(t(floor(t1(1)/dt):floor(t1(2)/dt)),z2(floor(t1(1)/dt):floor
(t1(2)/dt)), 'k');

grid on;

xlabel ('Time in s')
title ([char(int2str(listEq(i2))) ' ' char(listSt(i1)) ' BHZ'])
pause

z.b = 0;%t1(1)+z.b;
z.e = 1200;
z.npts = floor((1200/dt);
z.trace = z2;

% write in new directory

% create new dir
dir2 = [char(dirout) '/' char(int2str(listEq(i2))) ]
system(['mkdir ' char(dir2)])
fcutname = [char(dir2) '/' char(int2str(listEq(i2))) '.' 
char(listSt(i1)) '.BHZ.sac'];

writesac(z,char(fcutname));

```

```

    disp(['Eq =' char(int2str(i2)) ])
    disp(['St =' char(int2str(i1)) ])
    end
    close all
    end
end

% script pick Coda wave automatic for BHE.sac file

for i2=1:length(listEq)

    for i1=1:length(listSt)

        fname = [char(dir1) '/' char(int2str(listEq(i2))) '/'
char(int2str(listEq(i2))) '.' char(listSt(i1)) '.BHE.sac']

        if exist(char(fname), 'file') == 2

            z=readsac(char(fname));
            toto=filtfilt(a,b,z.trace);
            figure(1)
            plot(t(1:min([length(z.trace)
length(t)))),z.trace(1:min([length(t) length(z.trace)))));

            grid on;
            z.dist
            z.b

            % plot(t(1:min([length(z.trace)
length(t)))),toto(1:min([length(t) length(z.trace)])), 'r');
            % grid on;
            xlabel ('Time in s')
            title ([char(int2str(listEq(i2))) ' ' char(listSt(i1)) ' '
BHE'])
            hold on
            pause

            % pick coda (pick time of begin and end of coda length)

            % 2x surface wave arrival (vs ~3.5 km/s)
% t1(1)=3*z.dist/3.5;
% t1(2)=t1(1)+L_coda; % keep at least 800s of signal.
% if (z.e-t1(1)+z.b)>=L_coda

            % remove bad data
            t1(1)=z.dist/5;
            t2(1)=z.dist/2;

            [ia,ib]=max(abs(z.trace(floor(t1(1)/z.delta):floor(t2(1)/z.delta
))));

            % ib*z.delta;

            t1(1)=t1(1)+ib*z.delat;
            t1(2)=t1(1)+L_coda;

```

```

i=((floor(t1(1)/z.delta)):floor((t1(2)/z.delta)));

% [ia,ib]=max(abs(z.trace(1:floor(t1(1)/z.delta))));

ik = find(abs(z.trace(i))<ia);

if length(ik) < floor(L_coda/z.delta)
    disp('bad station!')
    disp(z.dist)
    continue
end

dt=z.delta;
z2=zeros(floor(2000/dt),1);

z2(i)=z.trace(i);
t2=t(i);

figure(2)
plot(t(i),z2(i));
grid on;

disp([int2str(floor(t1(2)/dt)-floor(t1(1)/dt))])

plot(t(floor(t1(1)/dt):floor(t1(2)/dt)),z2(floor(t1(1)/dt):floor(t1(2)/dt)), 'k');

grid on;

xlabel ('Time in s')
title ([char(int2str(listEq(i2))) ' ' char(listSt(i1)) ' BHE'])
pause

z.b = 0;%t1(1)+z.b;
z.e = 1200;
z.npts = floor((1200/dt);
z.trace = z2;

% write in new directory

% create new dir
dir2 = [char(dirout) '/' char(int2str(listEq(i2)))]
system(['mkdir ' char(dir2)])
fcutname = [char(dir2) '/' char(int2str(listEq(i2))) '.' char(listSt(i1)) '.BHE.sac'];

writesac(z,char(fcutname));

disp(['Eq =' char(int2str(i2)) ])
disp(['St =' char(int2str(i1)) ])
end
close all
end
end

```